ICAS 2021 SHANGHAI
International Council of the Aeronautical Sciences
32nd Congress of the International Council of the Aeronautical Sciences
September 6-10, 2021
Pudong Shangri-La, Shanghai, China

NASA-CRM LATERAL-DIRECTIONAL STABILITY DERIVATIVES COMPARISON BETWEEN SEMI-EMPIRICAL, VORTEX LATTICE AND PANEL METHOD

Rodrigo Sorbilli Cardoso de Sousa[1] & Roberto Gil Annes da Silva[2]

[1]PhD candidate at Instituto Tecnológico de Aeronáutica, rodrigosorbilli@gmail.com, +49 15730103853
[2]Professor at Instituto Tecnológico de Aeronáutica, gil@ita.br, +55 12997283884

Abstract

Aiming to build a 6DOF flight simulation model for NASA-CRM and, in the lack of experimental lateral-directional data, three different methodologies were assessed and compared: usual semi-empirical method based on historical wind tunnel experiments and first principals physics, vortex lattice method (using XFLR5 software), and panel method (using OpenVSP software). The comparison presented is exhaustive in the aspect of isolating each component aerodynamic contribution and presents a clear view of the agreement between the studied methodologies. This work serves as basis for a first assessment of the uncertainty of the stability derivatives, associated with each methodology, usually used during preliminary design of aircraft.

Keywords: Lateral-directional, stability, semi-empirical, vortex lattice, panel method

1. Introduction

This work was envisioned as part of the development of a 6DOF(degrees of freedom) model for the cruise condition of NASA-CRM aircraft to be used for academic purpose. As more data become available, which include now icing accretion and high-lift configuration, this “open source” aircraft becomes more relevant as a standard to be used by the academic community.

Semi-empirical method was set as the baseline method for estimating the lateral-directional derivatives, but the interest to understand what kind of agreement the lower fidelity numerical methodologies have with the semi-empirical one is an additional interesting research topic.

Regarding the numerical methodologies the goal was to use simple user standards, and not to aim for industrial or high-fidelity numerical simulations. In this aspect the open-source numerical software XFLR5 and OpenVSP were chosen. Especially OpenVSP is quite configurable, but aligned with the objectives of what a simple user can get from this kind of tools without too much tuning, the simulations used standard setting recommended by each software.

It is important to highlight that the results here presented does not represent limitations of the used methods or software. It is judged that more careful numerical simulation will achieve better results. Semi-empirical methods are used as the baseline for comparison. This decision was taken because the aircraft type and configuration is within the range of the method and reasonable agreement with real physics is expected for cruise configuration. Additionally, numerical simulations can be quite sensible to mesh and settings.

2. Defining the NASA CRM aircraft

The Common Research Model (CRM) was conceived at Langley Research Center and defined by a NASA-led group of U.S. aerodynamics leaders with detailed outer mold line design led by Boeing.

The purpose was to provide a modern, relevant standard and open geometry aircraft to also provide experimental data for the worldwide research community in order to validate and improve transonic computational fluid dynamics simulation of a modern transport aircraft. The first geometry included wing/body/nacelle/pylon/horizontal-tail in cruise configuration (flap not deflected) [1], [2], [3].
A wind tunnel model of the geometry was built and tested in NASA Ames 11-Ft Transonic Wind Tunnel [4][5], NASA NTF (National Transonic Facility) [7] [6], JAXA 2m x 2m Transonic Wind Tunnel (JTWT) [8] [9] [10] and European Transonic Windtunnel (ETW) [11].

The wind tunnel data encompass longitudinal runs (angle of attack sweep for zero angle of sideslip) of different configurations for Mach number from 0.20 to 0.92, and Reynolds number from 2 to 30 million. Although this data was generated for CFD validation and used in different Drag Prediction Workshop [12] [13], it is also useful for building a longitudinal flight dynamics model for studies of a modern transonic transport airplane dynamics. This model could be used for open and closed loop analysis, including the possibility to exercise the design a flight control law.

In terms of longitudinal modeling the available data lacks geometrical definition of the elevator and associated experimental results. This can be easily surpassed by defining a elevator based on similar aircraft types and using the experimental data of the horizontal tail along with numerical and semi-empirical methods to estimate the elevator control derivatives. In terms of lateral-directional the geometry lacks definition of ailerons, spoilers, vertical tail, rudder and associated experimental data. Aiming to develop a 6DOF flight dynamics model it was necessary to define the remaining geometries for NASA-CRM aircraft.

A vertical tail for the NASA-CRM model, based on 777-200 aircraft, was proposed by Atinault and Hue [14] aiming to build a wind tunnel model that was tested at ONERA S1MA and S2MA transonic wind tunnel facility [15], [16], [17]. In the present work, the proposed vertical tail was used for the NASA CRM model. Based on comparison of aircraft of the same class [18] the rudder was defined as 33% of the chord along the complete vertical tail span.

Regarding the aileron, the definition of the flaps along the wing span defines the inboard starting point of this control surface. Only outboard ailerons where considered. A high-lift CRM model used in the 3rd AIAA CFD High Lift Prediction Workshop, based on the NASA-CRM aircraft, was taken as a reference for the flaps definition. The flapped configuration was used to define the position of the retracted flap in the cruise configuration. The outboard flap ends at 72.3% of the semi-span. Taking this into account, and based on comparison of aircraft of the same class [18] the aileron was defined from 76% to 98% of the semi-span with 18% of local wing chord along its complete span.

The present work does not include spoilers because its intrinsic detached flow characteristics cannot be represented by the proposed numerical methodologies (vortex lattice and panel method). This variant of the NASA-CRM was named CRM-PEA[1] and the 3 views of the aircraft used in this study are presented in Figures 1, 2 and 3. The study was only accomplished for cruise configuration.

3. Evaluated methodologies

Three methodologies were chosen for evaluation:

1. Semi-empirical method.
2. Vortex Lattice (XFLR5) method.
3. Panel method (OpenVSP).

Although it is a physical inconsistency it was decided to decouple Mach number from Reynolds number in the methodologies for comparison purposes. Mach number = 0 was used for all methodologies,

[1] PEA stands for *Portal da Engenharia Aeronautica*, in Portuguese, meaning Aeronautical Engineering Hub. That is an aeronautical engineer training provider institution in Brazil.

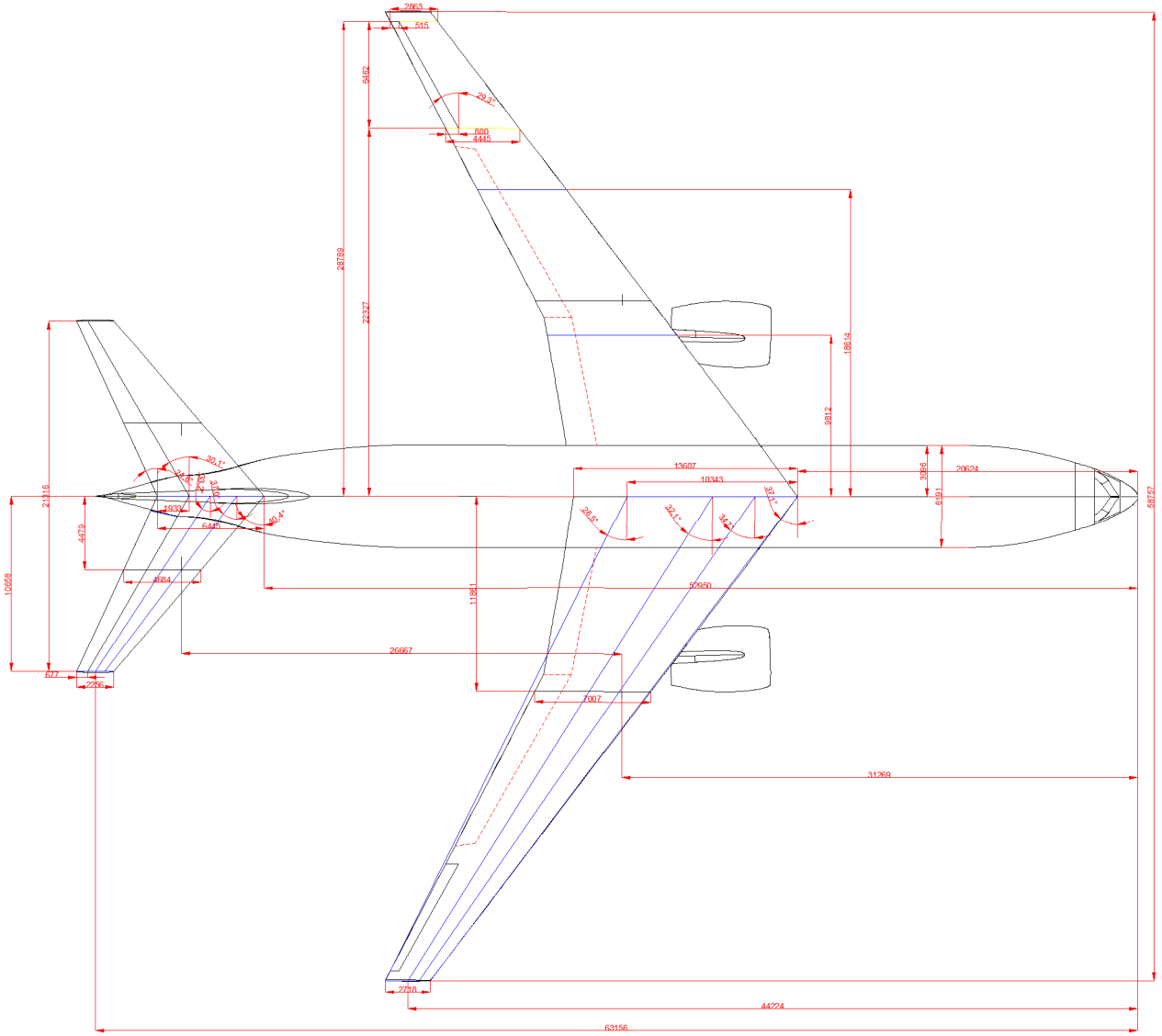

Figure 1 – CRM-PEA - Top View

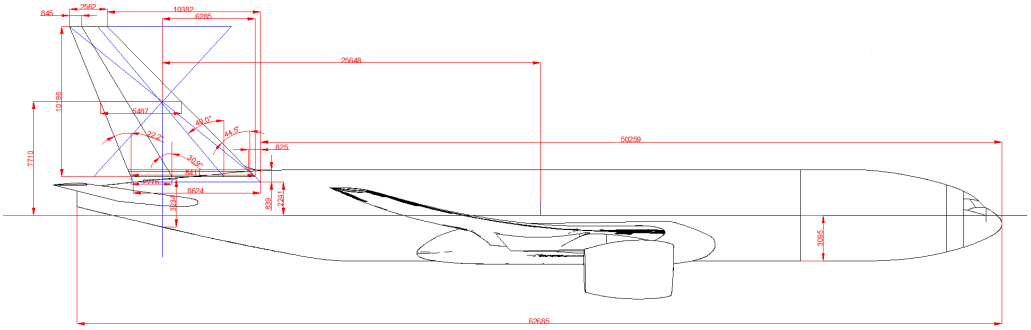

Figure 2 – CRM-PEA - Side View

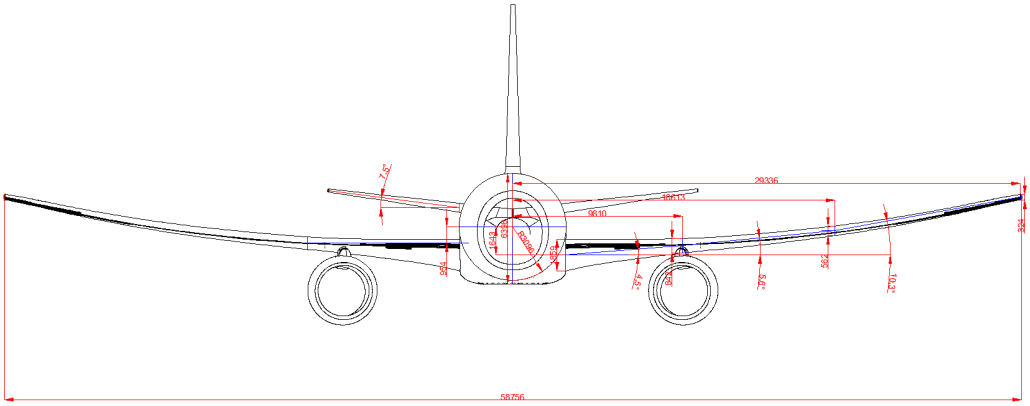

Figure 3 – CRM-PEA - Front View

and Reynolds number of 35 million was used in semi-empirical and XFLR5. OpenVSP panel method is fully potential, so there is no Reynolds number effect. Wing reference area was used for determination of the coefficients. Stability axis was used for all methods and the necessary conversions were applied to numerical methodologies results. In order to provide the breakdown of the effects for the comparison with the semi-empirical methodology, several configurations were simulated in the numerical methodologies: W, WB, WBV, WV, WVH, WBVH, and V[2]. For both numerical cases mesh convergence studies were performed for WBVH and WVH configurations. The mesh properties used in mesh convergence study for both methodologies are presented in Table 1 and 2.

Table 1 – XFLR5 - Vortex Lattice + Panel method (only fuselage) meshes

	Wing			Fuselage			VT			HT		
Mesh name	Span	Chord	Total	Length	Circumference	Total	Span	Chord	Total	Span	Chord	Total
Ultra-low	46	10	460	40	20	800	23	10	230	46	10	460
Low	64	15	960	40	20	800	32	15	480	64	15	960
Medium	96	20	1920	40	40	1600	48	20	960	96	20	1920
High	96	50	4800	60	80	4800	48	50	2400	96	50	4800

Table 2 – OpenVSP - Panel method meshes

	Wing			Fuselage			VT			HT		
Mesh name	Span	Chord	Total	Length	Circumference	Total	Span	Chord	Total	Span	Chord	Total
Low	50	21	1664	40	20	1464	25	21	1064	50	21	1984
Medium	104	53	9344	60	81	7120	50	21	2064	102	21	4064
High	104	81	14384	153	81	22000	50	49	4976	102	49	9776

The airfoil of 9 sections along the semi-wingspan were extracted from the NASA-CRM CAD geometry in order to build the geometry for the numerical analysis (Figure 4). For the horizontal and vertical tail 2 sections were taken, being it the root and tip sections. For the fuselage, 14 cross sections were taken along its length (Figure 5).

3.1 Semi-empirical method

The book Aircraft Design of Jan Roskam [18] was taken as the reference for the semi-empirical method. It presents a compilation of several other references and selection of relevant effects according to the author experience. Most of the methods proposed by Roskam are exactly the same or have similarity to DATCOM [19] and/or NASA semi-empirical methodologies [20].

Although the methodology herein applied considers the angle of attack as a variable, it is applicable only for low angle of attack, compatible with cruise condition.

[2]W-wing, B-body, H-horizontal tail, V-vertical tail

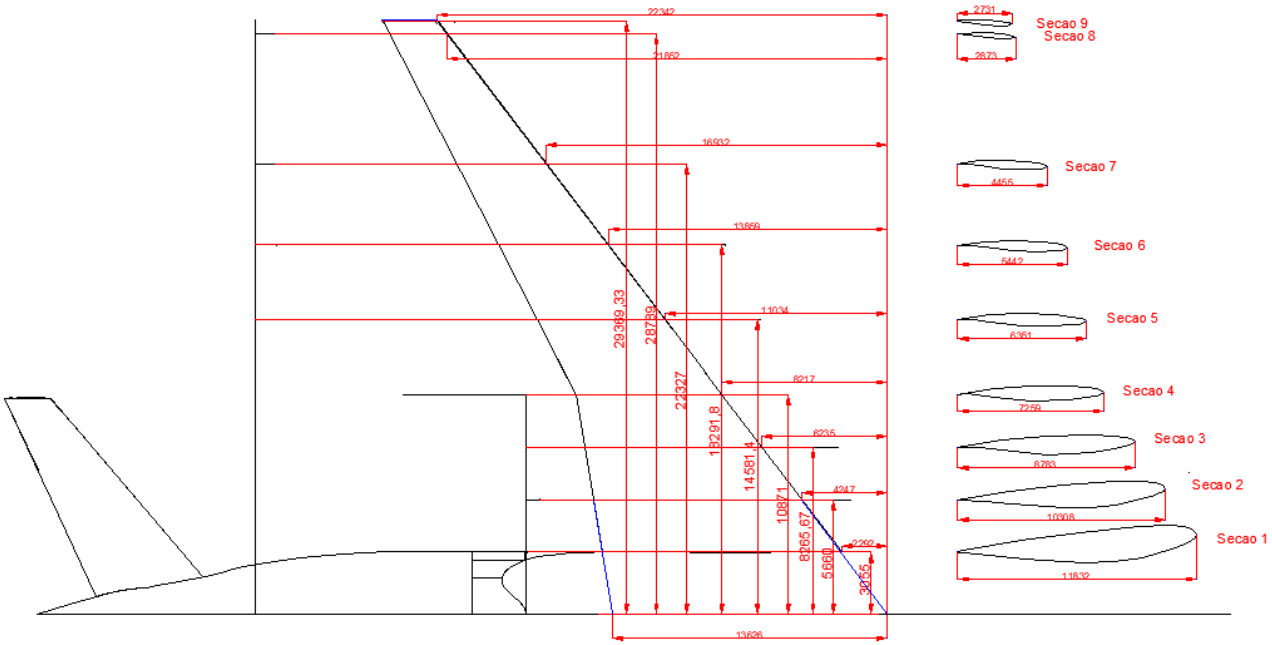

Figure 4 – Wing sections used to build the geometry in numerical methodologies

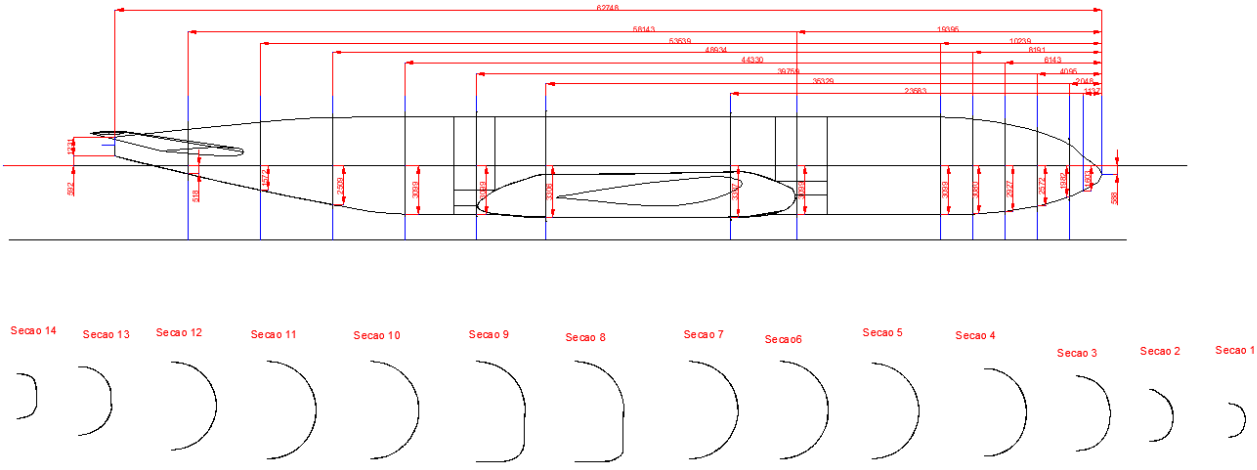

Figure 5 – Fuselage sections used to build the geometry in numerical methodologies

3.2 Aerodynamic numerical simulation restrictions

The aim of the study is to present what is attainable to obtain in low fidelity numerical simulations using open-source codes (XFLR5 and OpenVSP). The size of the meshes were constrained in time by about 8 minutes per simulated point using a standard notebook (Intel 4 Core i7-8550U CPU @ 1.80GHz with 24GB of RAM memory).

3.3 Vortex Lattice method

The vortex lattice method was assessed using the software XFLR5(v6.47). The method is not a pure potential vortex lattice method because the 2D data of the airfoil is interpolated in respect to the local angle of attack from a previous generated databank using an embedded XFoil code [22]. This means that this methodology has a bi-dimensional representation of the viscosity in the lifting surfaces, through the XFoil integral boundary layer methodology. In any case, tridimensional effects in boundary layer are not taken into account. The nominal Reynolds number used in the simulations was 35 million, referenced to the mean aerodynamic chord, defined at the aircraft cruise condition.

Although not recommended by the software, the fuselage, by means of panel method, was also included in the relevant configurations together with the vortex lattice simulation of the lifting surfaces. The “high” mesh of the configuration WBVH is presented in Figures 6 and 7.

Because XFLR5 runs dynamic derivatives only with vortex lattice method, the dynamic derivatives were simulated for WVH configuration.

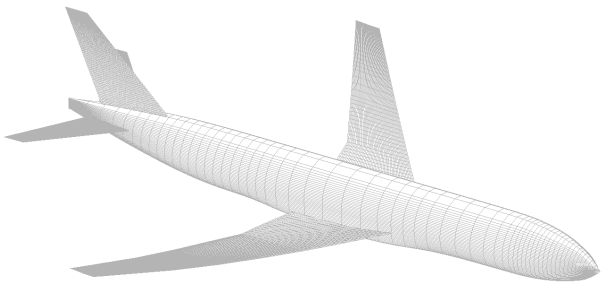

Figure 6 – XFLR5 - Iso view of “high” mesh

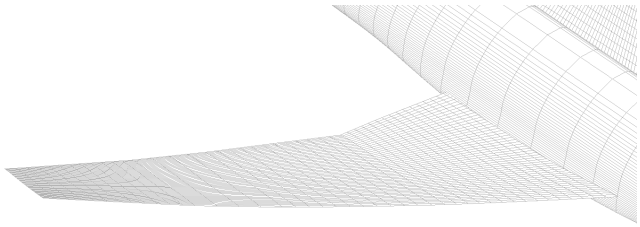

Figure 7 – XFLR5 - Iso view zoom of “high” mesh

3.4 Panel method

The panel method was assessed using the OpenVSP(3.21.2) software [21]. All the surfaces, lifting and non-lifting ones, were simulated by panel method and no viscosity is considered in the methodology. The simulations considered 64 nodes for the flexible wake and a standard number of 5 iterations for the wake. The “high” mesh of the configuration WBVH is presented in Figures 8 and 9.

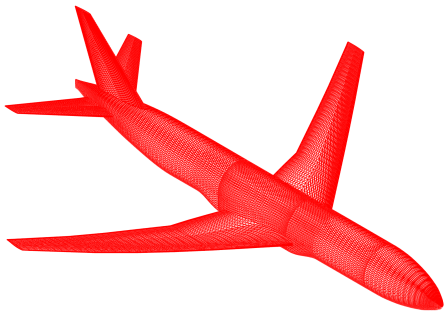

Figure 8 – OpenVSP - Iso view of “high” mesh

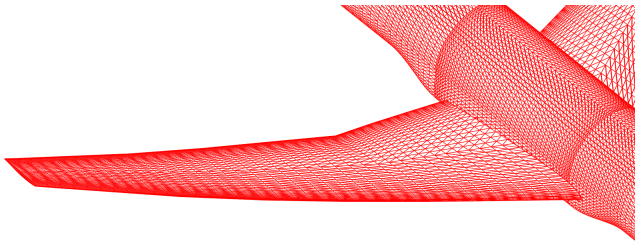

Figure 9 – OpenVSP - Iso view zoom of “high” mesh

3.5 Numerical methods test matrix

The semi-empirical method usually provides a breakdown of contribution of each aircraft component. For the numerical methods the simulation test matrix was defined in order to provide such breakdown by the comparison of different configurations. This test matrix is presented in Table 3, it consists of 153 numerical simulation points. The simulation was executed in terms of angle of attack (Alpha) sweep (0°, 5° and 10°) for two different sideslip angle (Beta), 0° and 5°. The stability derivatives were obtained by linear approximation using the 2 simulated sideslip angles for each angle of attack. For the control surfaces, aileron and rudder, the simulations were only performed for Beta = 0° and the control derivatives obtained by linearization of the simulated deflections. Control derivatives were only simulated in the vortex lattice method.

Table 3 – Numerical methods test matrix

Configuration	Software	Mesh	Alpha[°]	Beta[°]	Aileron[°]	Rudder[°]	N° of Points
W							
W	XFLR5	High	0,5,10	0, 5	0	0	6
W	OpenVSP	High	0,5,10	0, 5	0	0	6
WB							
WB	XFLR5	High	0,5,10	0, 5	0	0	6
WB	OpenVSP	High	0,5,10	0, 5	0	0	6
WBV							
WBV	XFLR5	High	0,5,10	0, 5	0	0	6
WBV	OpenVSP	High	0,5,10	0, 5	0	0	6
WV							
WV	XFLR5	High	0,5,10	0, 5	0	0	6
WV	OpenVSP	High	0,5,10	0, 5	0	0	6
WBVH							
WBVH	XFLR5	Ultra-low	0,5,10	0, 5	0	0	6
WBVH	XFLR5	Low	0,5,10	0, 5	0	0	6
WBVH	XFLR5	Medium	0,5,10	0, 5	0	0	6
WBVH	XFLR5	High	0,5,10	0, 5	0	0	6
WBVH	OpenVSP	Low	0,5,10	0, 5	0	0	6
WBVH	OpenVSP	Medium	0,5,10	0, 5	0	0	6
WBVH	OpenVSP	High	0,5,10	0, 5	0	0	6
WVH							
WVH	XFLR5	Ultra-low	0,5,10	0, 5	0	0	6
WVH	XFLR5	Low	0,5,10	0, 5	0	0	6
WVH	XFLR5	Medium	0,5,10	0, 5	0	0	6
WVH	XFLR5	High	0,5,10	0, 5	0	0	6
WVH	OpenVSP	Low	0,5,10	0, 5	0	0	6
WVH	OpenVSP	Medium	0,5,10	0, 5	0	0	6
WVH	OpenVSP	High	0,5,10	0, 5	0	0	6
V							
V	XFLR5	High	0,5,10	0, 5	0	0	6
V	OpenVSP	High	0,5,10	0, 5	0	0	6
Aileron							
W	XFLR5	High	0,5,10	0	+10, -10	0	6
Rudder							
WVH	XFLR5	High	0,5,10	0	0	+10	3

4. Results

4.1 Mesh convergence

It is recognized that the mesh convergence study herein presented (Table 1 and 2) is not complete in terms of assessing individually the effect of different variables in the mesh, as the number of chord and span elements, and number of panels in the fuselage and other variables were usually changed at the same time. The aim was to consistently increase all the number of panels during the mesh definition to create different resolution meshes.

XFLR5 - Vortex Lattice + panel method (fuselage)

For the vortex lattice method (XFLR5) the mesh distribution of the fuselage is automatically generated by the software and the use of fuselage with the panel method is not recommended by the software. Although problems of the interface between the lifting surfaces, using vortex lattice method, and the fuselage, using panel method, are expected, the goal was to evaluate how far those problems affect the overall results.

Because of this expected problem of the fuselage representation the mesh convergence is presented with and without the fuselage (Figures 10 and 11 respectively). The convergence is presented as the relative percentage value of the lateral-directional stability derivatives in respect to the “high” mesh configuration.

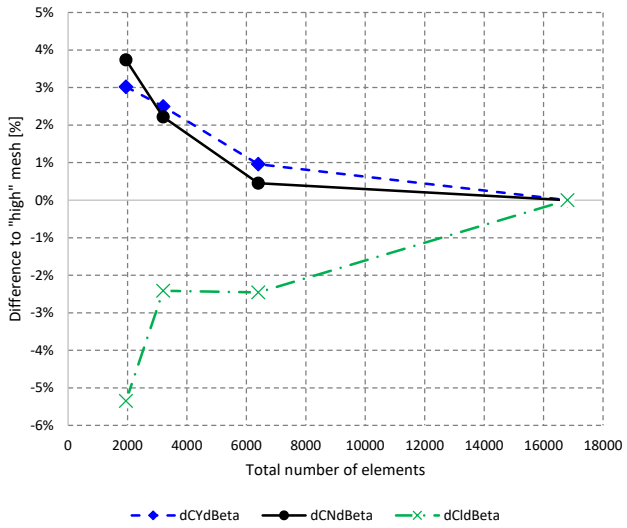

Figure 10 – XFLR5 - WVBH - Mesh convergence

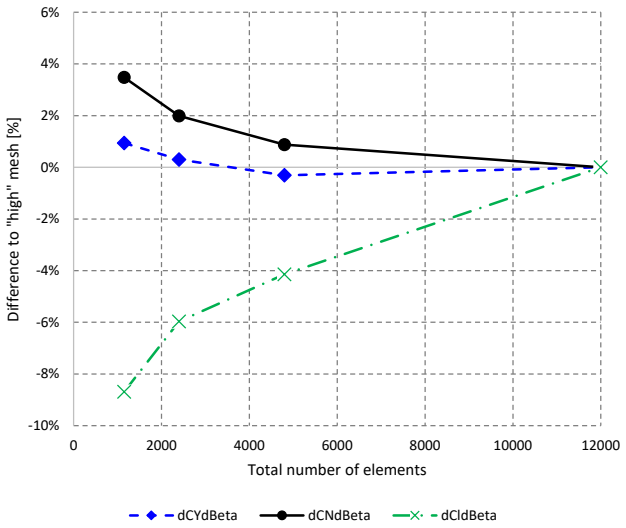

Figure 11 – XFLR5 - WVH - Mesh convergence

The overall trend of convergence with the increased number of elements presented in Figures 10 and 11 for WBVH and WVH is similar and satisfactory for all stability derivatives. Even for the “Ulta-low” resolution mesh the differences are within $\pm$ 10 $\%$. For the “Medium” mesh configuration differences for $C_{Y\beta}$ and $C_{N\beta}$ are within 1% and 4% for $C_{l\beta}$.

Although no higher fidelity mesh than the named “high” one is presented, the convergence is satisfactory in terms of relative difference between meshes. The maximum number of the elements were also constrained by the amount of simulations required for the work, associated with the solving time using a standard notebook. It is also important to highlight that XFLR5 presented convergence problems for higher resolution meshes in the fuselage.

OpenVSP - Panel method

The mesh convergence for WBVH and WVH is presented in Figures 12 and 13 respectively. The configuration with fuselage shows large differences between the meshes, the difference between the “Medium” and “High” meshes are within $\pm$ 15%, but the $C_{N\beta}$ in the order of -70% is not satisfactory. Constrained by computational limitations the decision was not include a higher resolution mesh and continue the study with the already defined “high” mesh.

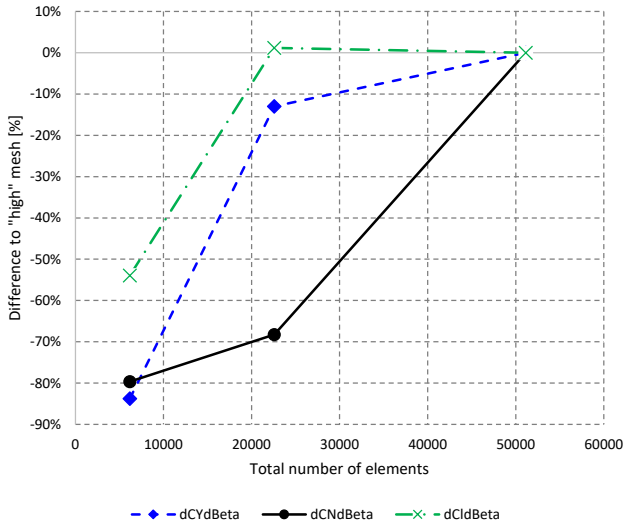

Figure 12 – OpenVSP - WBVH - Mesh convergence

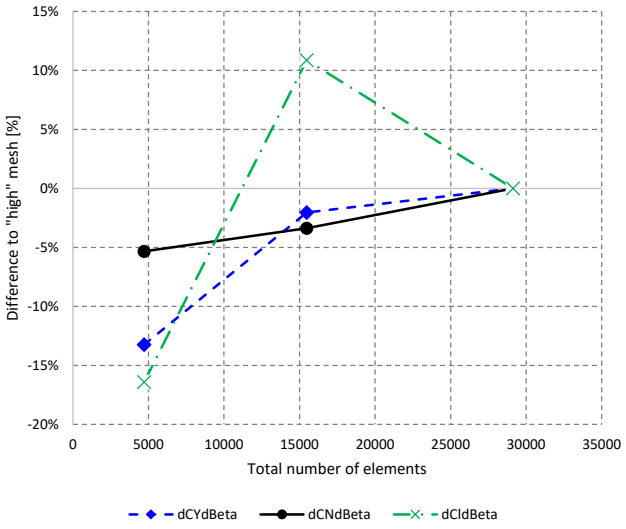

Figure 13 – OpenVSP - WVH - Mesh convergence

For the WVH configuration the overall difference during the convergence study is better than for WBVH. For the “low” mesh the differences are within $\pm$ 16 % and within $\pm$ 11 % for the “medium” one. Differently than the XFLR5 convergence, the trend indicates that a higher resolution mesh could improve the results significantly, especially for the WBVH configuration.

4.2 Numerical X Semi-empirical

The results are presented for the “high” resolution mesh for both numerical methods. Two graphs are presented for each stability or control derivative:

- Absolute value.
- Relative percentage difference in respect to semi-empirical method.

There are 3 blocks of results in each graph:

- 1 - Alpha = 0°.
- 2 - Alpha = 5°.
- 3 - Alpha = 10°.

In the next topics the presented numerical methods are referenced only by the name of the software used: XFLR (section 3.3) and OpenVSP (section 3.4).

The agreement level between the numerical and semi-empirical methods were set as:

- Good: within $\pm$15%.

- Reasonable: within ±30%.
- Bad: higher than ±30%.

$C_{Y\beta}$

The $C_{Y\beta}$ is presented for the following aircraft components:

- Wing ($C_{Y\beta W}$).
- Fuselage ($C_{Y\beta B}$).
- Wing-fuselage ($C_{Y\beta WB}$).
- Vertical tail ($C_{Y\beta V}$).
- Wing - vertical tail - horizontal tail ($C_{Y\beta WVH}$).
- Complete aircraft ($C_{Y\beta WBVH}$).

$C_{Y\beta W}$

Results are presented in Figures 14 and 15. Other than the reasonably good agreement between semi-empirical and OpenVSP at Alpha = 0° (8%) the differences between methodologies is high. It is important to highlight that the wing contribution to the complete aircraft $C_{Y\beta}$ is small. Semi-empirical method does not account for angle of attack effect in this stability derivative.

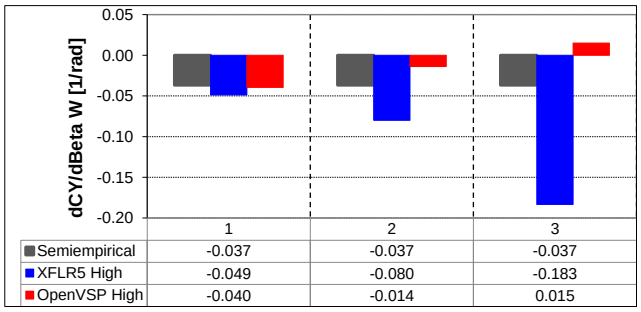

Figure 14 – $C_{Y\beta W}$

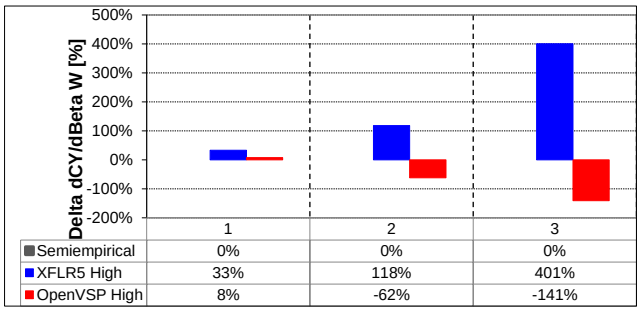

Figure 15 – $\Delta\, C_{Y\beta W}$

$C_{Y\beta B}$

The fuselage contribution is directly obtained in the semi-empirical method. For the numerical methods the fuselage contribution was defined as the difference between the WBVH and WVH configuration. For XFLR5 results of WBVH only converged at Alpha = 0°, so the other angles of attack are not presented. Results are presented in Figures 16 and 17. Differences observed are high and even have opposite value than the differences already seen in the wing alone case. This is indicating that the adequate simulation of the side force of the fuselage in the used numerical simulations is challenging.

$C_{Y\beta WB}$

The constant angle of attack $C_{Y\beta WB}$ of the semi-empirical method has a better agreement with the numerical methodologies as the angle of attack is increased (Figures 18 and 19). For Alpha = 0° the differences are in the order of 80% and decrease to 27% at Alpha = 10°.

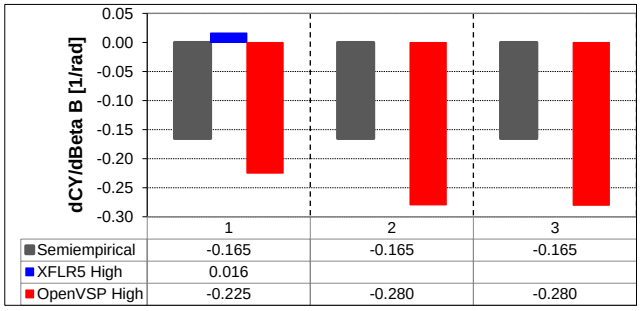

Figure 16 – $C_{Y\beta B}$ - B=WBVH-WVH

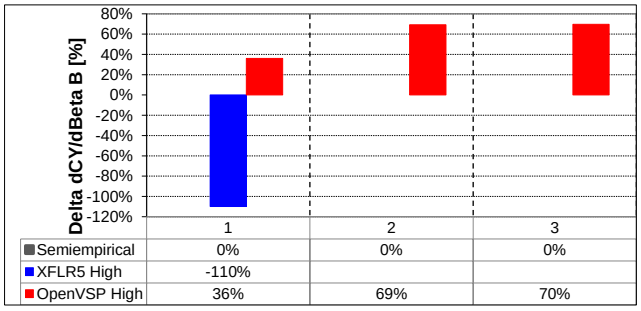

Figure 17 – $\Delta\, C_{Y\beta B}$ - B=WBVH-WVH

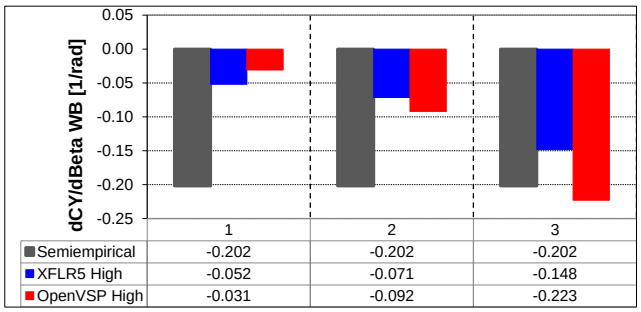

Figure 18 – $C_{Y\beta WB}$

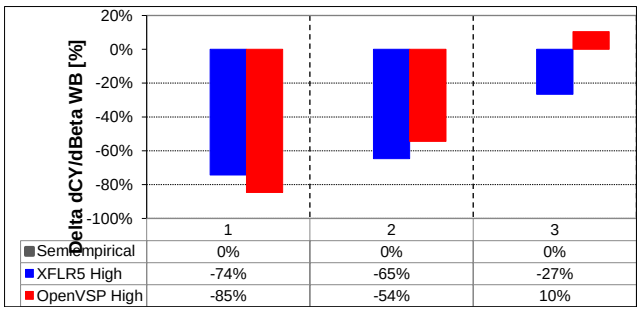

Figure 19 – $\Delta\, C_{Y\beta WB}$

$C_{Y\beta V}$

The vertical tail results are presented for the difference between the WV and W configurations (Figures 20 and 21). The numerical results are within $\pm$15% in respect to the semi-empirical method, except at Alpha = 10°. It shall be noted that the fuselage effect in the vertical tail was not considered in semi-empirical method for this comparison, as the fuselage is not present in the numerical simulation.

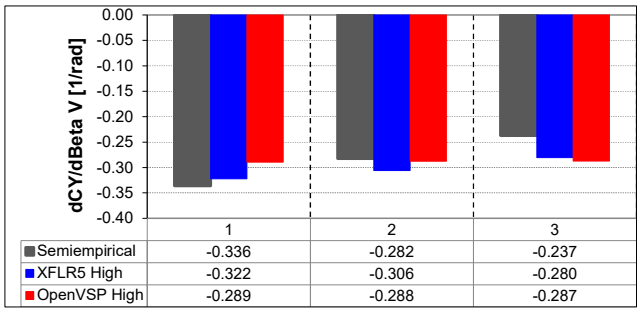

Figure 20 – $C_{Y\beta V}$ - V=WV - W

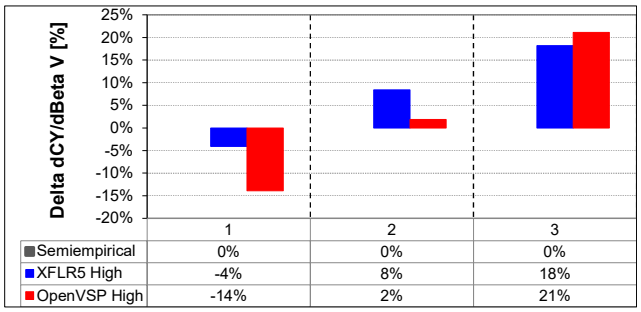

Figure 21 – $\Delta\, C_{Y\beta V}$ - V=WV - W

$C_{Y\beta WVH}$

The configuration without the fuselage is presented because the fuselage can be the source of aerodynamics differences in numerical methods. In Figures 22 and 23 it can be seen a good agreement of OpenVSP for all angles of attack. XFLR5 has a good agreement for Alpha = 0°, but the angle of attack effect presents a different trend than the other methodologies. This effect was already seen in the isolated wing and is also present in this configuration.

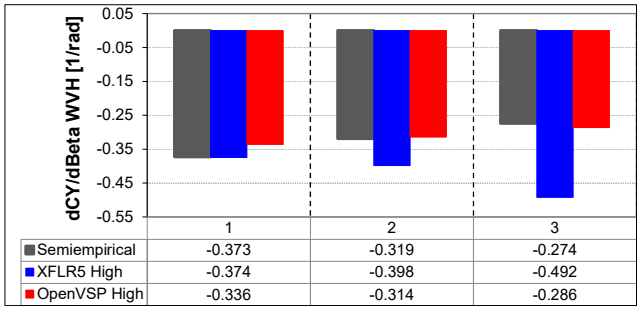

Figure 22 – $C_{Y\beta WVH}$

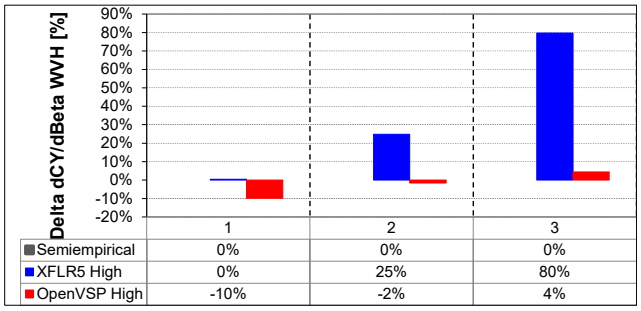

Figure 23 – $\Delta\, C_{Y\beta WVH}$

$C_{Y\beta WBVH}$

In Figures 26 and 27 the absolute values and relative percentage difference in respect to the semi-empirical methodology are presented, being 1 for Alpha 0°, 2 for Alpha 5° and 3 for Alpha 10°. For this configuration XFLR5 only converged in the sideslip cases for Alpha = 0°. The results show a good agreement between OpenVSP and semi-empirical and a bad agreement of XFLR5. As depicted in the component's breakdown before, the fuselage effect in XFLR5 is not adequately captured.

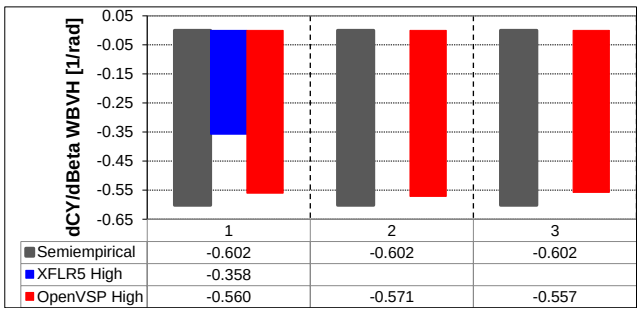

Figure 24 – $C_{Y\beta WBVH}$

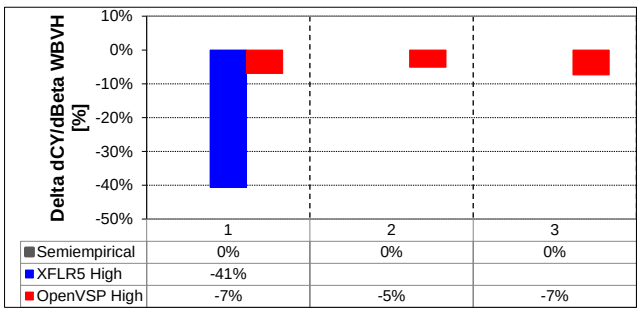

Figure 25 – $\Delta\, C_{Y\beta WBVH}$

The difference in the aircraft components contribution is clear in Figures 26 and 27 that presents the relative contribution of WB and VH to the $C_{Y\beta WBVH}$ at Alpha = 0. In Figure 27 1 stand for wing-fuselage, 2 for tail, being the values the contribution of each component to the overall stability derivative. In this case, the tail effect was obtained considering the fuselage for numerical methodologies (VH = WBVH - WB). The vertical tail of numerical methods is overestimated in respect to the semi-empirical and the wing-fuselage contribution is underestimated.

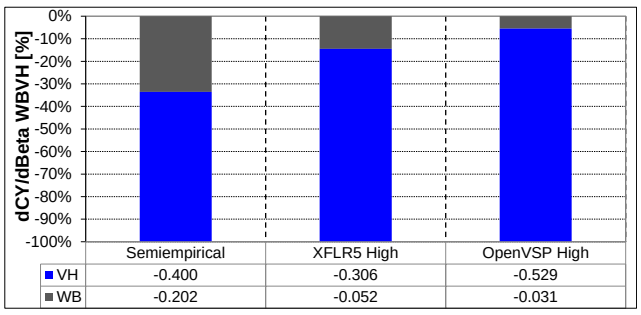

Figure 26 – $C_{Y\beta WBVH}$ - Contribution - Alpha = 0°

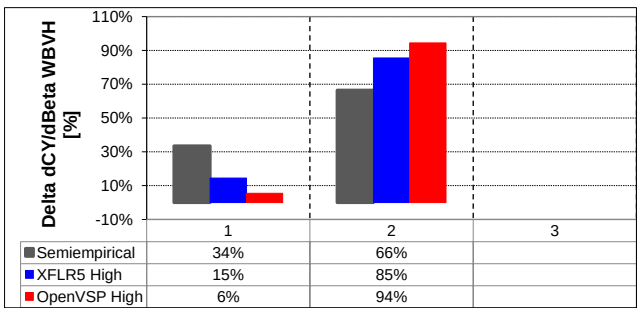

Figure 27 – $\Delta\, C_{Y\beta WBVH}$ - Contribution - Alpha = 0°

$C_{N\beta}$

The $C_{N\beta}$ is presented for the following aircraft components:

- Wing ($C_{N\beta W}$).
- Fuselage ($C_{N\beta B}$).
- Wing-fuselage ($C_{l\beta WB}$).
- Vertical tail ($C_{N\beta V}$).
- Wing - vertical tail - horizontal tail ($C_{N\beta WVH}$).
- Complete aircraft ($C_{N\beta WBVH}$).

$C_{N\beta W}$

The semi-empirical methodology applied is focused on cruise condition, low angle of attack, and the effect of the wing in $C_{N\beta}$ is neglected. As there is no semi-empirical reference for this parameter only the absolute values are presented in Figure 28. As prescribed by the semi-empirical method the numerical methodologies indicate negligible $C_{N\beta W}$ at Alpha 0° and larger values at higher angles of attack. Large differences between numerical methodologies occur at Alpha = 10°, XFLR5 results are about 78% larger than OpenVSP.

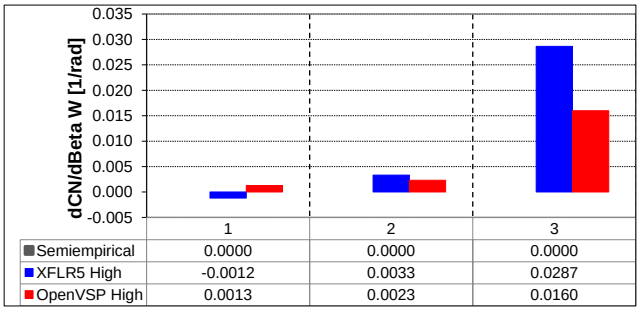

Figure 28 – $C_{N\beta W}$

$C_{N\beta B}$

The fuselage contribution is directly obtained in the semi-empirical method. For the numerical methods the fuselage contribution was defined as the difference between the WBVH and WVH configuration. XFLR5 result is limited to Alpha = 0°. OpenVSP presents a reasonable agreement (-20%) with semi-empirical methodology while XFLR5 result is significantly off.

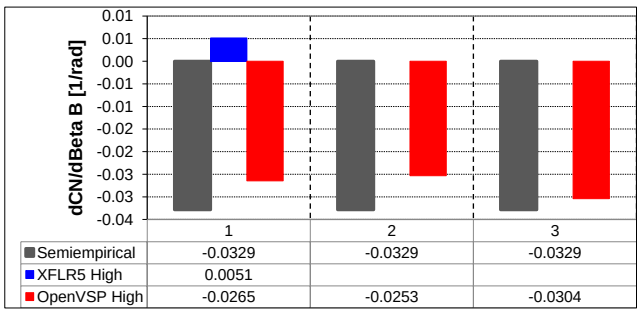

Figure 29 – $C_{N\beta B}$ - B=WBVH-WVH

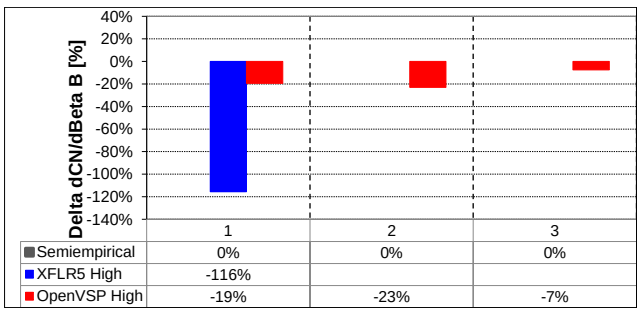

Figure 30 – Δ $C_{N\beta B}$ - B=WBVH-WVH

$C_{N\beta V}$

For the numerical methods the $C_{N\beta V}$ was obtained by the subtraction of WV by the W configuration. The fuselage effect in the vertical tail was not considered for the semi-empirical method. OpenVSP

presents a constant offset of about -15% and XFLR5 presents a larger angle of attack effect that makes it loose agreement at larger angles.

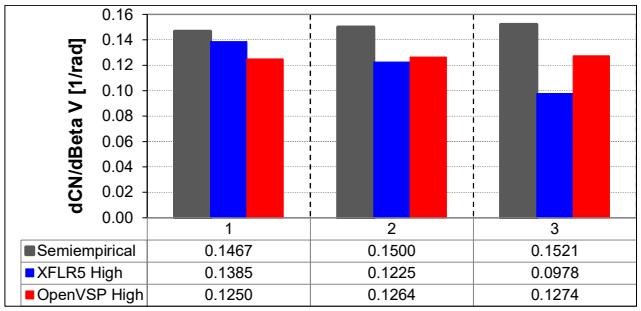

Figure 31 – $C_{N\beta V}$ - V=WV-W

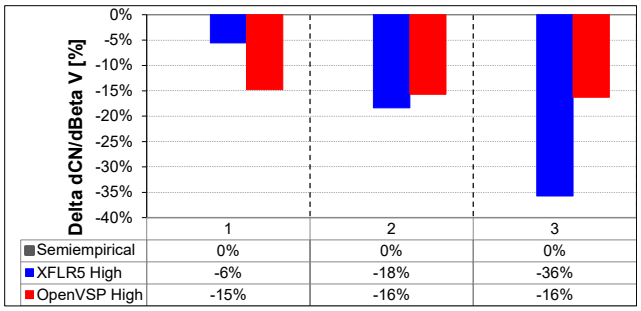

Figure 32 – $\Delta\, C_{N\beta V}$ - V=WV-W

$C_{N\beta WVH}$

Numerical results presented a good agreement with semi-empirical methodology, within $\pm$14%, as can be seen in Figures 33 and 34.

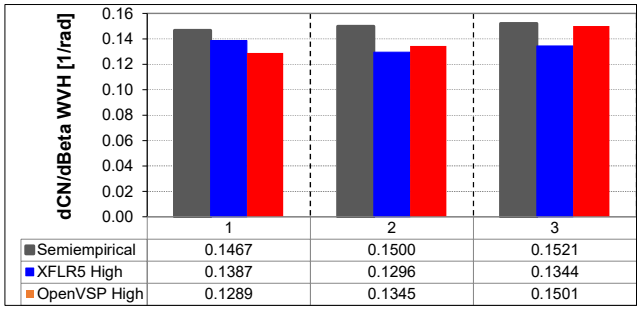

Figure 33 – $C_{N\beta WVH}$

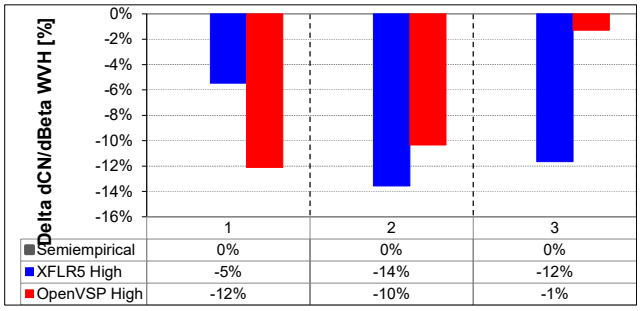

Figure 34 – $\Delta\, C_{N\beta WVH}$

$C_{N\beta WBVH}$

In Figures 35 and 36 the absolute values and percentage difference in respect to the semi-empirical method are presented. XFLR5 closely matches the semi-empirical method at Alpha = 0°, similarly to the WVH result. OpenVSP is off by -28% at Alpha = 0°. The decrease in the agreement in respect to the WVH configuration, from -12% to -28%, may indicate that the fuselage is the source of the discrepancy. OpenVSP difference decreases with angle of attack but is still off by about -19%. at Alpha = 10°.

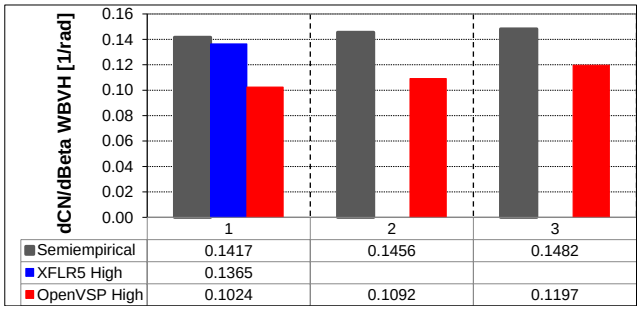

Figure 35 – $C_{N\beta WBVH}$

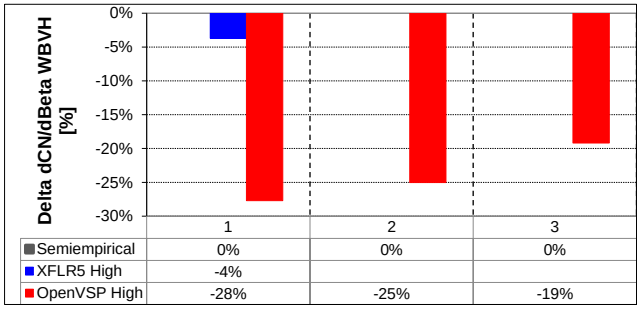

Figure 36 – $\Delta\, C_{N\beta WBVH}$

In Figure 37 the contribution of the tail, wing and fuselage is presented for each methodology. In

Figure 38 is presented the relative contribution of each component in respect to the overall derivative for Alpha = 0°. 1 stands for wing-fuselage, 2 for tail. Numerical methodologies overestimate the tail contribution in respect to the semi-empirical.

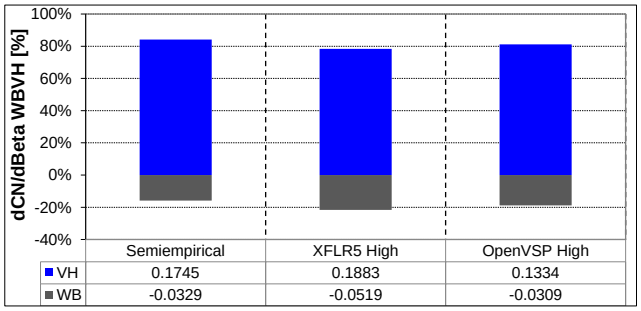

Figure 37 – $C_{N\beta WBVH}$ - Contribution - Alpha = 0°

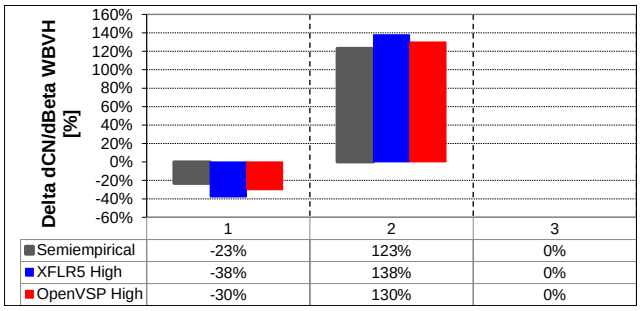

Figure 38 – $\Delta\, C_{N\beta WBVH}$ - Contribution - Alpha = 0°

$C_{l\beta}$

The $C_{l\beta}$ is presented for the following aircraft components:

- Wing ($C_{l\beta W}$).
- Fuselage ($C_{l\beta B}$).
- Wing-fuselage ($C_{l\beta WB}$).
- Vertical tail ($C_{l\beta V}$).
- Horizontal tail ($C_{l\beta H}$).
- Wing - vertical tail - horizontal tail ($C_{l\beta WVH}$).
- Complete aircraft ($C_{l\beta WBVH}$).

$C_{l\beta W}$

Figures 39 and 40 presents results for of the wing for $C_{l\beta}$. It is important to highlight that for this derivative the angle of attack of the semi-empirical method was interpolated to match the C_{LW} of the numerical methodologies, that presented a close match of this parameter. XFLR5 has a good agreement with semi-empirical in the order of -9% to +4% while OpenVSP presents differences in the range of +14% to +29%.

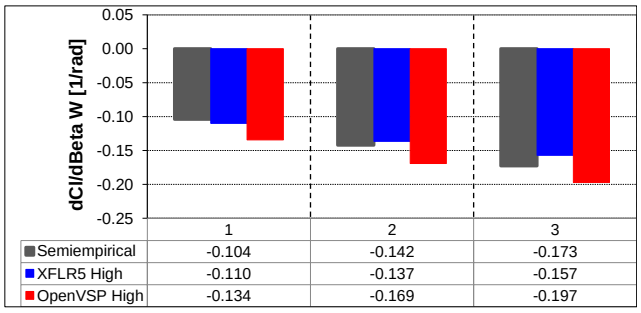

Figure 39 – $C_{l\beta W}$

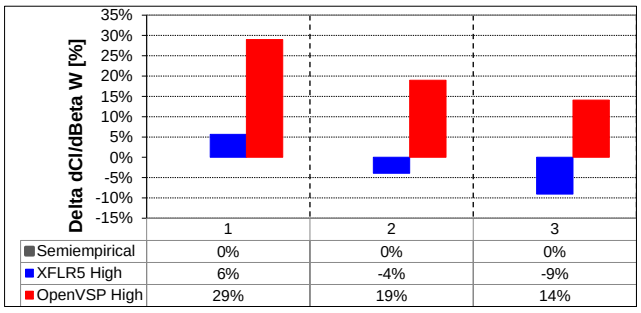

Figure 40 – $\Delta\, C_{l\beta W}$

$C_{l\beta B}$

For all methodologies, including the semi-empirical, the fuselage contribution to $C_{l\beta}$, that is mainly in terms of effect in the wing by modification of the local angle of attack in the wing root, was obtained by the subtraction of the WBVH by WVH configuration. XFLR5 results are limited to Alpha = 0° as previously commented.

As presented in Figures 41 and 42, XFLR5 captures reasonably the effect of the fuselage in the wing, with a difference of -16% to the semi-empirical methodology, while OpenVSP presents very large differences. The mesh convergence study, presented in section 4.1 indicates that the main reason for such discrepancy is the numerical problems associated with the WVH geometry. The better results of OpenVSP for $C_{l\beta WBVH}$ supports this theory.

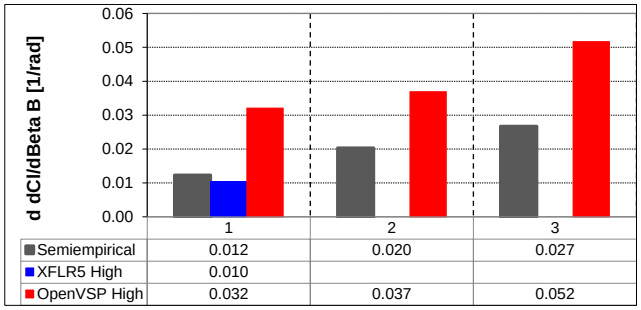

Figure 41 – $C_{l\beta B}$ - B=WBVH-WVH

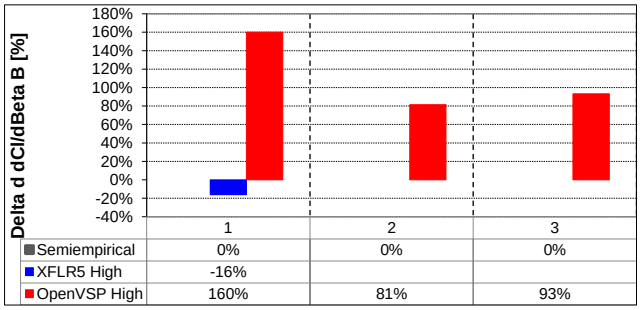

Figure 42 – $\Delta\, C_{l\beta B}$ - B=WBVH-WVH

$C_{l\beta WB}$

Results for wing-fuselage configuration are presented in Figures 43 and 44. OpenVSP presents a better agreement with semi-empirical methodology that improves with angle of attack. XFLR5 overestimates $C_{l\beta WB}$ by about 20%.

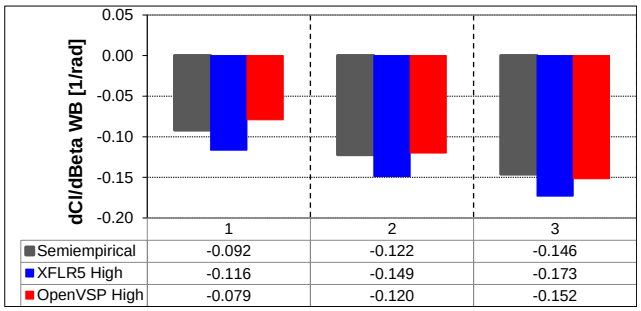

Figure 43 – $C_{l\beta WB}$

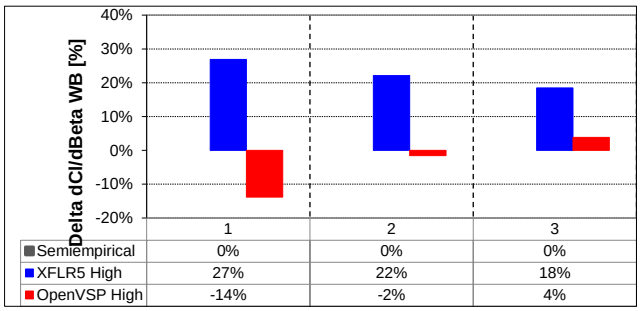

Figure 44 – $\Delta\, C_{l\beta WB}$

$C_{l\beta V}$

For the numerical methods the $C_{l\beta V}$ was obtained by the subtraction of WV by the W configuration. Fuselage effect in the vertical tail was not considered for the semi-empirical method. At Alpha = 0° there is an offset of -11% for XFLR5 and -22% for OpenVSP. The numerical methodologies capture the trade of angle of attack effect, but it is largely overestimated by XFLR5, leading to larger percentage values in higher angles of attack. The percentage analysis is also affected by the fact that the derivative of the reference (semi-empirical) decreases in value with angle of attack.

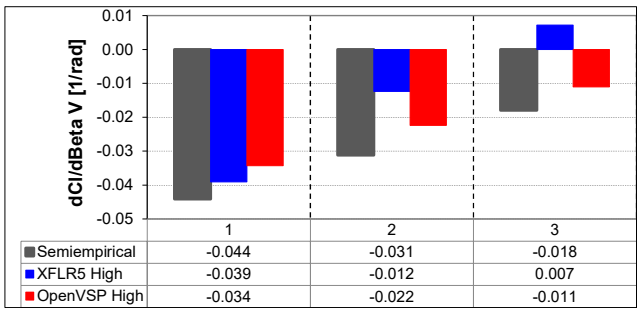

Figure 45 – $C_{l\beta V}$ - V=WV-W

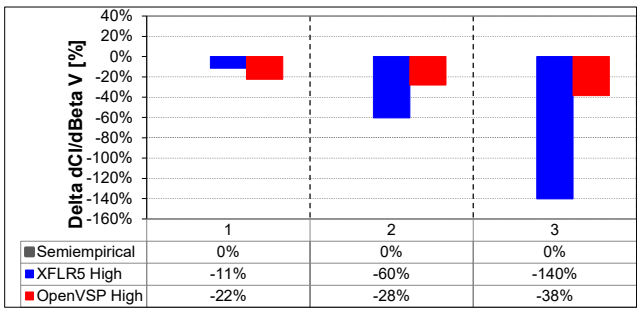

Figure 46 – $\Delta\, C_{l\beta V}$ - V=WV-W

$C_{l\beta H}$

The effect of horizontal tail is about 3% of the total $C_{l\beta}$, and although the differences presented in Figures 47 and 48 are large, the impact in the total derivative is small.

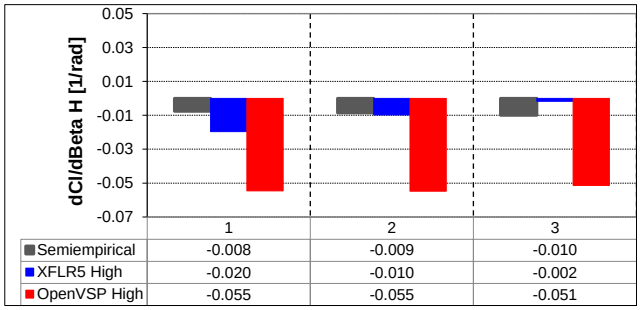

Figure 47 – $C_{l\beta H}$

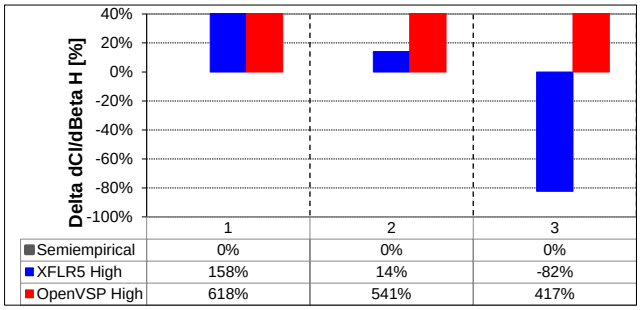

Figure 48 – $\Delta\, C_{l\beta H}$

$C_{l\beta WVH}$

Results considering only the lifting surfaces are presented in Figures 49 and 50. OpenVSP overestimates the angle of attack effect, possibly because of the potential flow nature of the panel method used. The lack of mesh convergence for this configuration may also play a role. For Alpha = 0° it presents a difference of 9% in respect to semi-empirical, and this difference increases with angle of attack. XFLR5 captures the angle of attack effect in agreement to the semi-empirical methodology, but has a offset of about 8% for all angles of attack.

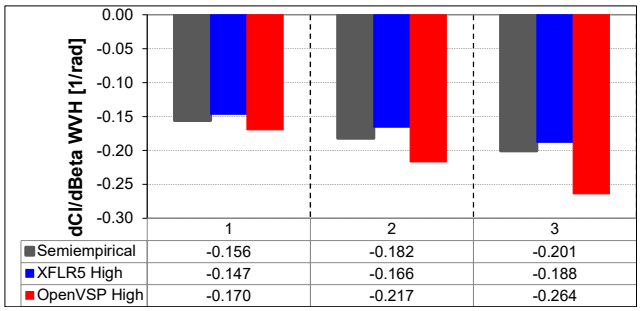

Figure 49 – $C_{l\beta WVH}$

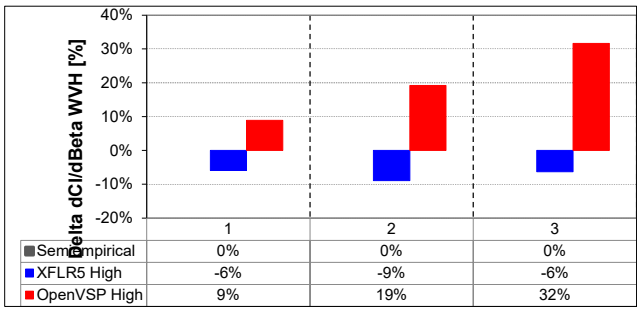

Figure 50 – $\Delta\, C_{l\beta WVH}$

$C_{l\beta WBVH}$

For the total lateral stability derivative, although it has been presented larger differences in components, the results are good (Figures 51 and 52). The larger difference is for XFLR5 at Alpha = 0°,

-13%. Results from OpenVSP are good for Alpha = 0° and reach a maximum of +7% at Alpha = 10°.

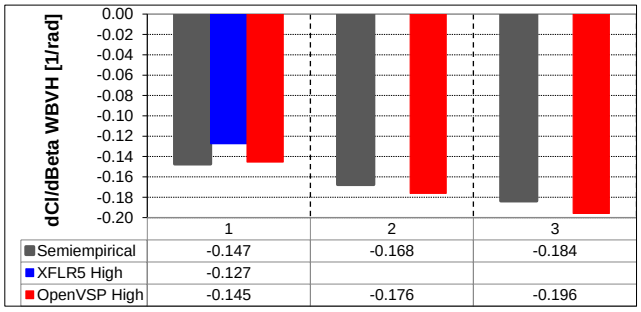

Figure 51 – $C_{l\beta WBVH}$

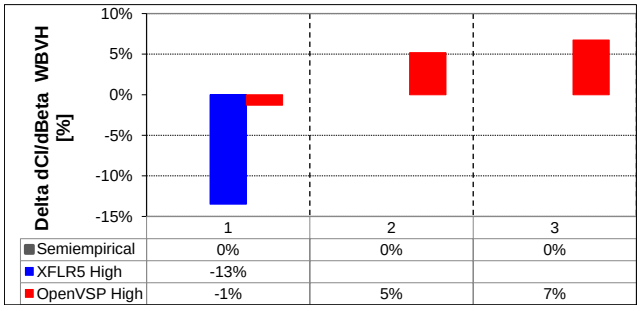

Figure 52 – $\Delta\, C_{l\beta WBVH}$

In Figure 53 the contribution is grouped in WB and VH for Alpha = 0°. OpenVSP presents a better distribution of the effect in respect to the semi-empirical methodology than XFLR5. In Figure 54 the group 1 is related to WB and 2 to the VH contribution for Alpha = 0°. It is clear that although XFLR5 has captured the overall derivative within 13% in respect to the semi-empirical method, the contribution of each component does not agree.

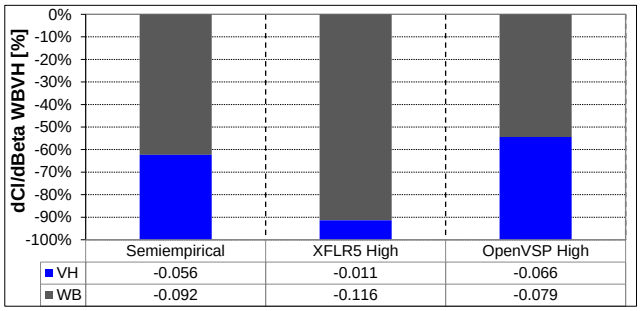

Figure 53 – $C_{l\beta WBVH}$ - Contribution - Alpha = 0°

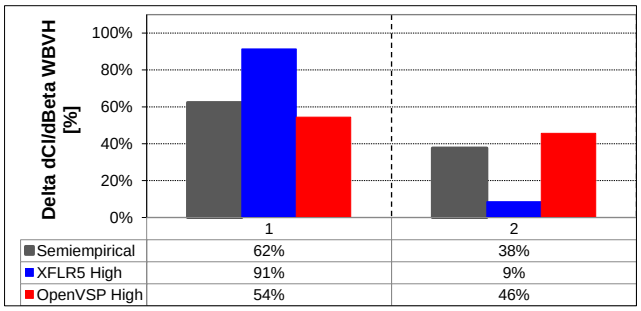

Figure 54 – $\Delta\, C_{l\beta WBVH}$ - Contribution - Alpha = 0°

Dynamic derivative - p (roll rate)

C_{Yp}

In Figures 55 and 56 it is presented the contribution of vertical tail to the C_{Yp}. Only OpenVSP and semi-empirical methods are presented, due to the XFLR5 limitations discussed in section 3.3 The agreement between methodologies is good at Alpha = 0° and OpenVSP largely overestimates the effect of angle of attack for the higher values.

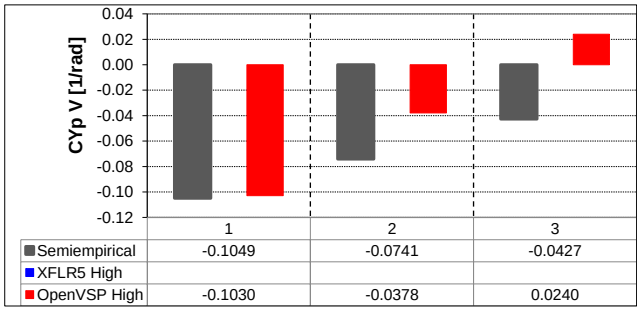

Figure 55 – C_{YpV}

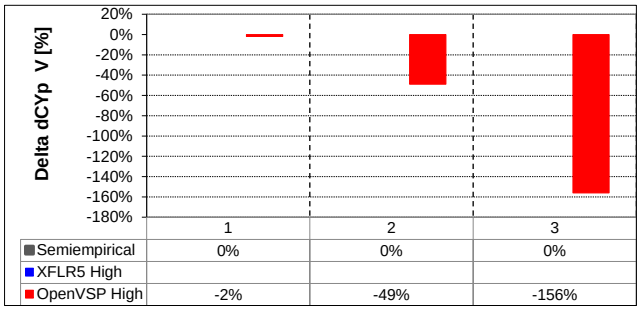

Figure 56 – $\Delta\, C_{YpV}$

In Figures 57 and 58 it is presented the derivative of the complete aircraft for the three methodologies.

It is important to highlight that the simulations in XFLR5 are for WVH configuration and WBVH for in OpenVSP. Only Alpha = 0° is available for XFLR5. Both comments apply to all dynamic derivatives.

At Alpha = 0° XFLR5 presents -15% than the semi-empirical and OpenVSP -43%. For higher angles of attack the absolute and relative difference of OpenVSP increases to large values.

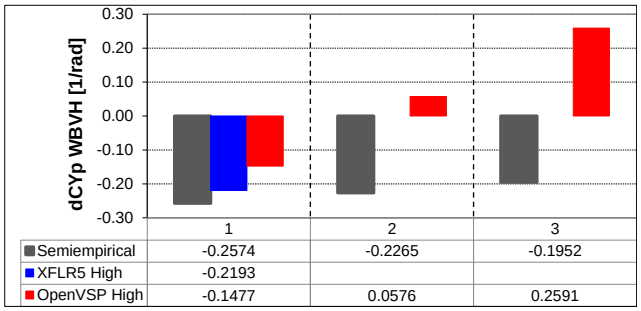

Figure 57 – C_{YpWBVH}

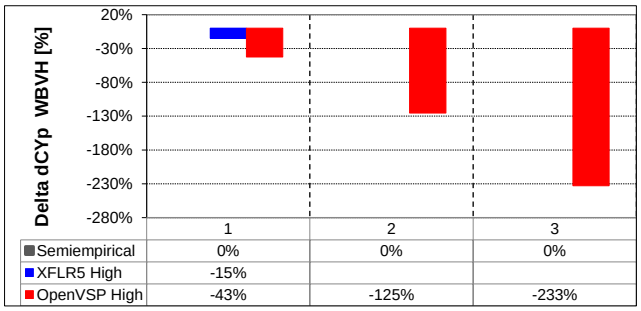

Figure 58 – $\Delta\, C_{YpWBVH}$

C_{Np}

The vertical tail contribution in C_{Np} is presented in Figures 59 and 60. There is a good agreement between methodologies at Alpha =0°, but as seen in C_{Yp} the differences increases with angle of attack. In this case OpenVSP effect decreases less than the values of the semi-empirical method.

For the complete aircraft, Figures 61 and 62, XFLR5 largely overestimates the derivative at Alpha =0°, while the agreement of OpenVSP is reasonable at low angle of attack and decreases with the increase of it. It is important to highlight that this is not a main dynamic derivative and the impacts in flight simulation of the aircraft are judged to be small.

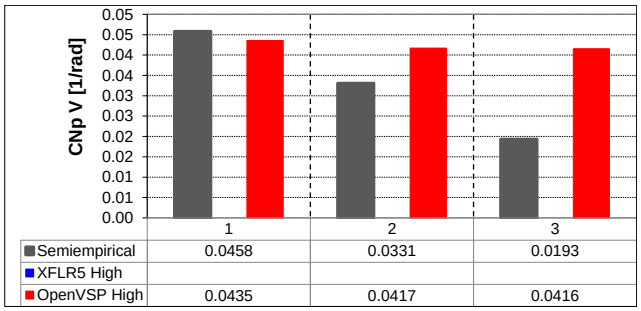

Figure 59 – C_{NpV}

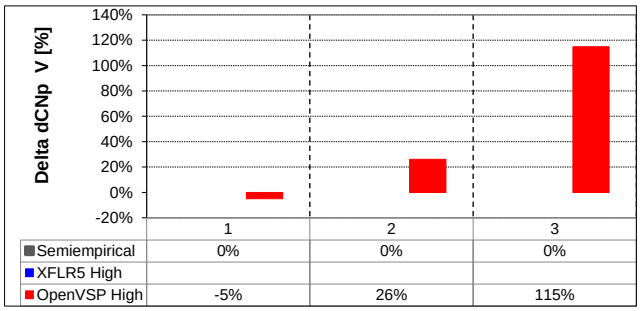

Figure 60 – $\Delta\, C_{NpV}$

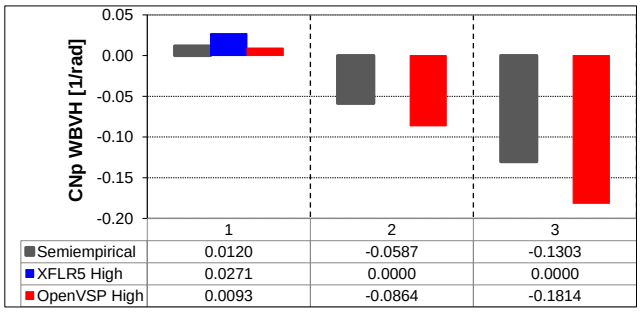

Figure 61 – C_{NpWBVH}

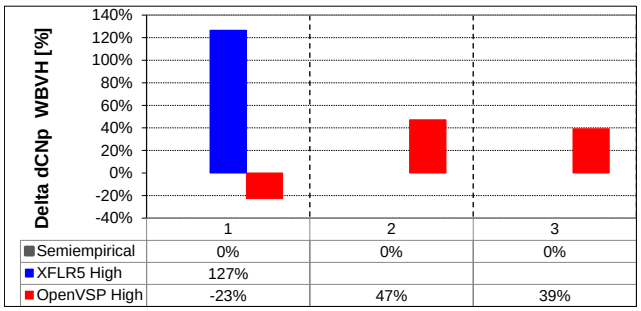

Figure 62 – $\Delta\, C_{NpWBVH}$

C_{lp}

C_{lp} is one of the main dynamic derivatives. In Figures 63 and 64 the vertical tail contribution is presented with reasonable agreement at Alpha =0° and large differences for larger angles of attack as seen for other dynamic derivatives.

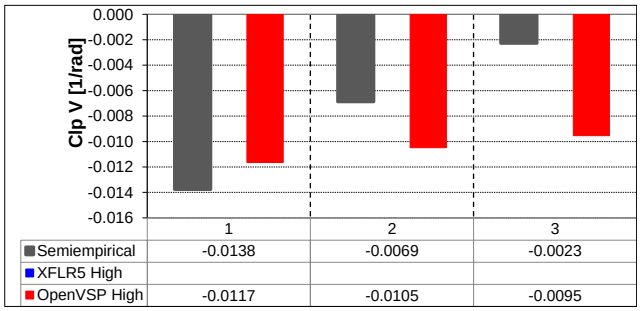

Figure 63 – C_{lpV}

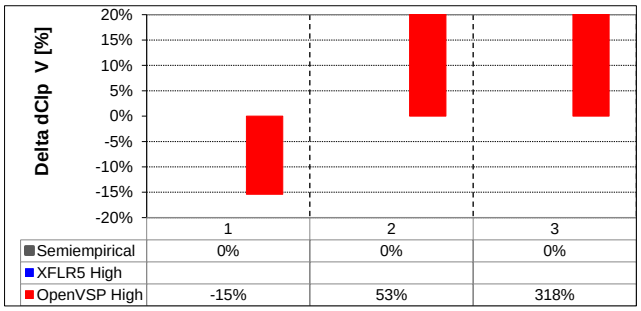

Figure 64 – $\Delta\, C_{lpV}$

Considering the complete aircraft at Alpha = 0° (Figures 65 and 66) the agreement between methodologies is good. OpenVSP presents the same good agreement at higher angles of attack.

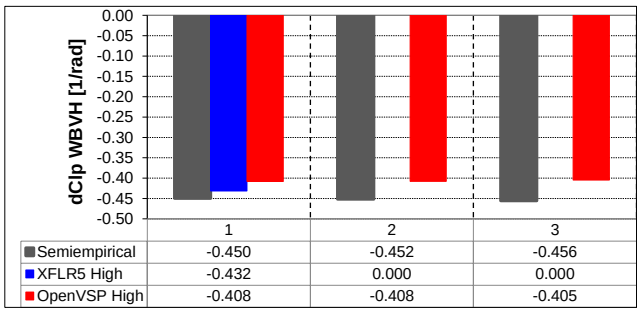

Figure 65 – C_{lpWBVH}

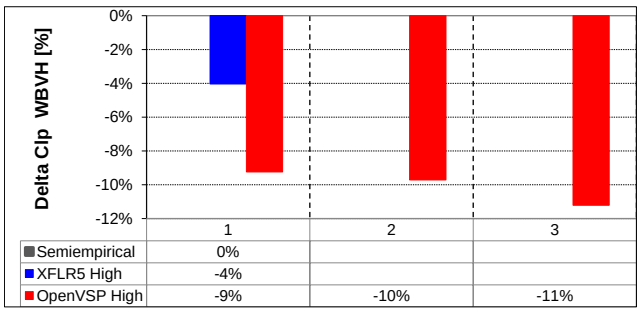

Figure 66 – $\Delta\, C_{lpWBVH}$

Dynamic derivative - r (yaw rate)

C_{Yr}

C_{Yr} together with C_{Nr} are one of the main dynamic derivatives in respect to yaw rate. The comparison for the complete aircraft C_{Yr} is presented in Figures 67 and 68. XFLR5 presents the same good agreement seen in C_{lp}, but OpenVSP underestimates the derivative in the order of -25% for all angles of attack.

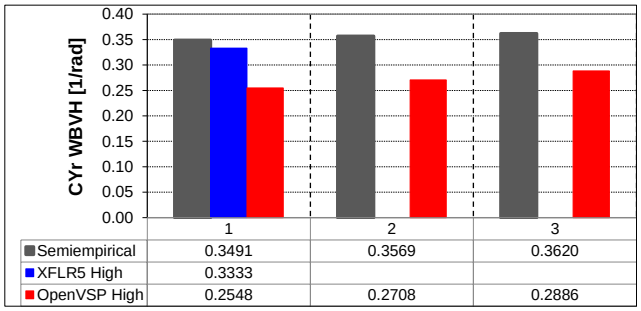

Figure 67 – C_{YrWBVH}

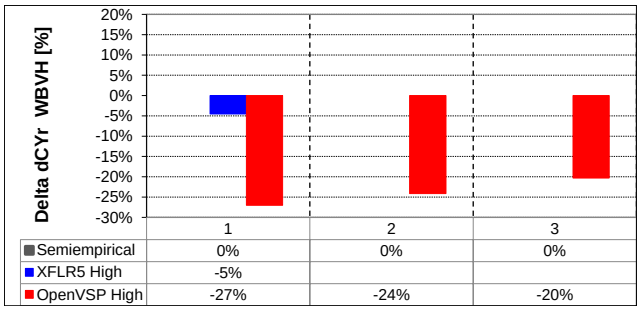

Figure 68 – $\Delta\, C_{YrWBVH}$

C_{Nr}

In Figures 69 and 70 the comparison between C_{Nr} for the three methodologies is presented. All methodologies have a good agreement for Alpha = 0°, with XFLR5 presenting results more similar to semi-empirical. OpenVSP maintain the same order of difference with increasing angle of attack.

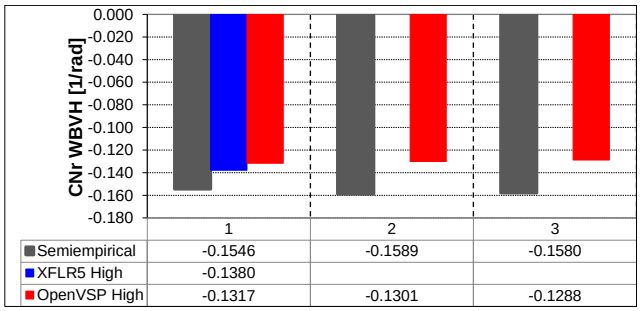

Figure 69 – C_{NrWBVH}

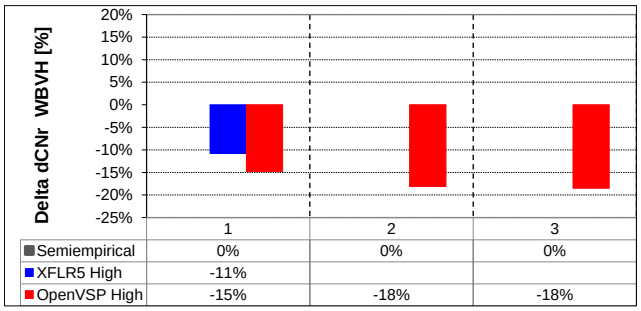

Figure 70 – $\Delta\, C_{NrWBVH}$

C_{lr}

For C_{lr} the discrepancies between methodologies is higher, as can be seen in Figures 71 and 72. Both numerical methodologies underestimate the semi-empirical values with a significant difference (about -50%). As commented for C_{Np}, the impact of this difference in the flight simulation of the aircraft is judged to be small.

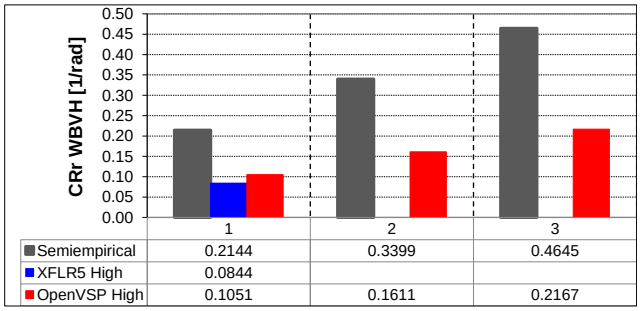

Figure 71 – C_{lrWBVH}

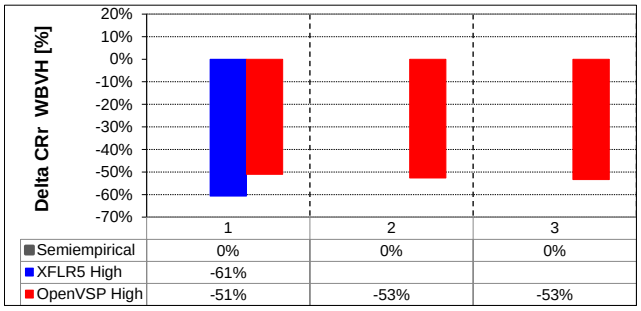

Figure 72 – $\Delta\, C_{lrWBVH}$

Aileron

Aileron effect were simulated only in vortex lattice method (XFLR5) for the isolated wing configuration. The derivative was obtained by the linear approximation of -10°, 0° and +10° of aileron deflection. For semi-empirical methodology there is no angle of attack effect in $C_{laileron}$, so the same value is presented for all.

The results are presented in Figures 73 and 74. XFLR5 overestimates the aileron effect by about +40% in respect to semi-empirical method for all angles of attack.

Regarding $C_{Naileron}$, presented in Figures 75 and 76, the differences are large and the angle of attack effect for this secondary control derivative is opposite between the methodologies.

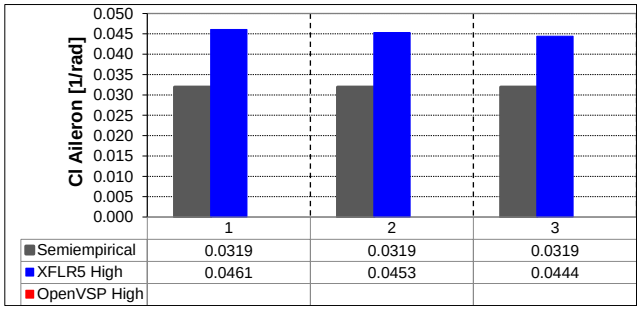

Figure 73 – $C_{laileron}$

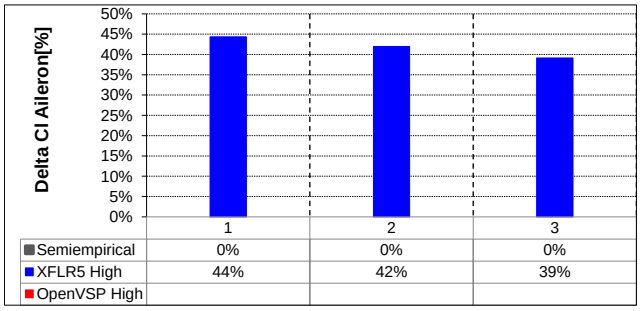

Figure 74 – $\Delta\, C_{laileron}$

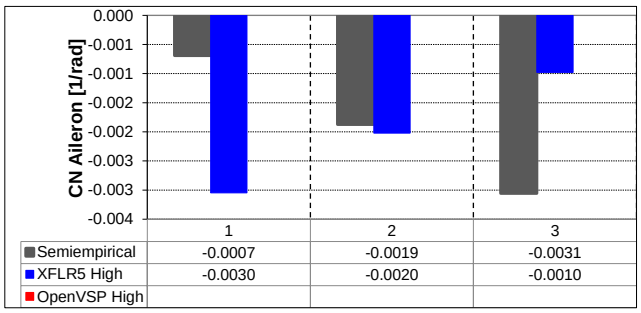

Figure 75 – $C_{Naileron}$

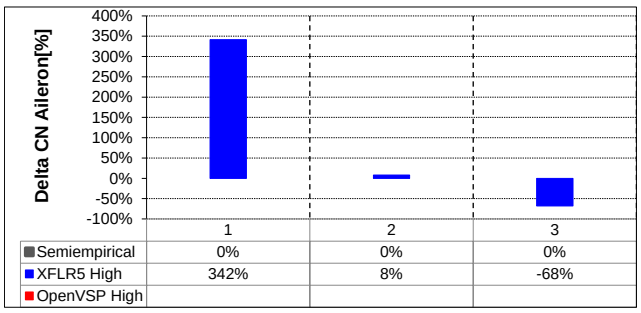

Figure 76 – $\Delta\, C_{Naileron}$

Rudder

Rudder deflection +10° was simulated in XFLR5, WVH configuration. The results for $C_{Nrudder}$ are presented in Figures 77 and 78. There is a good agreement at Alpha = 0° with 12% difference. The difference increases with angle of attack to 25% as both methodologies indicate opposite effect of angle of attack.

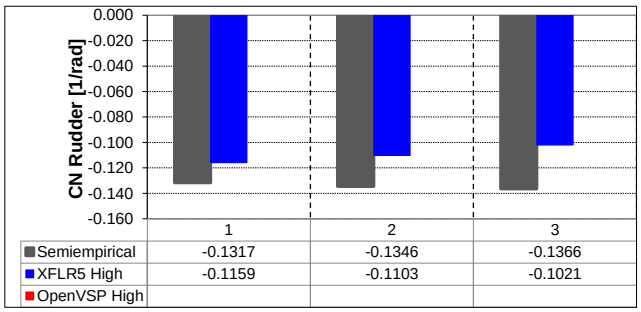

Figure 77 – $C_{Nrudder}$

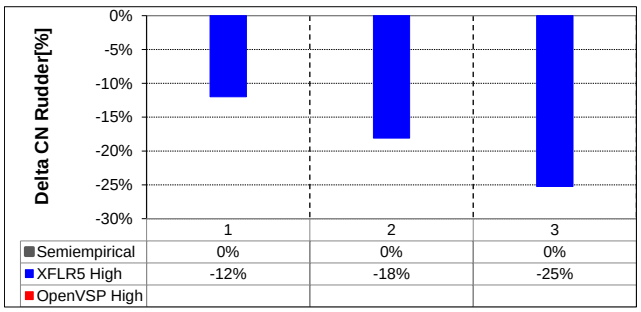

Figure 78 – $\Delta\, C_{Nrudder}$

For the $C_{lrudder}$ the difference is larger at Alpha = 0°, 33%, with XFLR5 underestimating the effect in respect to the semi-empirical at Alpha = 0° and overestimating the angle of attack effect, as presented in Figures 79 and 80.
A summary of the results is presented in Figure 81. The agreement level between the numerical and semi-empirical methods were set as:

- Good: within ±15%.
- Reasonable: within ±30%.
- Bad: higher than ±30%.

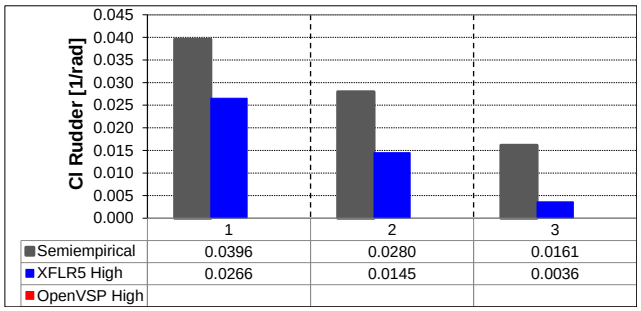

Figure 79 – $C_{lrudder}$

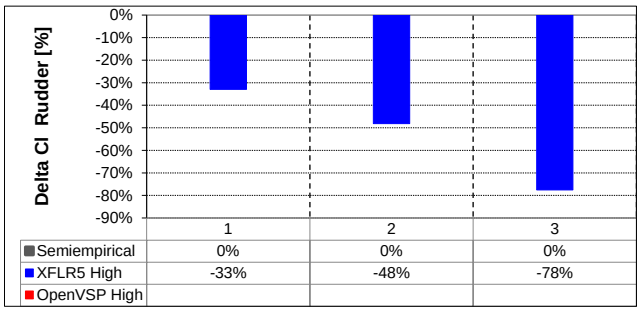

Figure 80 – $\Delta\, C_{lrudder}$

	Stability derivatives		
	Alpha	XFLR5	OpenVSP
CYbeta W	0°	bad	good
	5°	bad	bad
	10°	bad	bad
CYbeta B	0°	bad	bad
	5°	bad	bad
	10°	bad	bad
CYbeta WB	0°	bad	bad
	5°	bad	bad
	10°	reasonable	good
CYbeta V	0°	good	good
	5°	good	good
	10°	reasonable	reasonable
CYbeta WVH	0°	good	good
	5°	reasonable	good
	10°	bad	good
CYbeta WBVH	0°	bad	good
	5°		good
	10°		good
Clbeta W	0°	good	reasonable
	5°	good	reasonable
	10°	good	good
Clbeta WB	0°	reasonable	good
	5°	reasonable	good
	10°	reasonable	good
dClbeta B	0°	reasonable	bad
	5°		bad
	10°		bad
Clbeta H	0°	bad	bad
	5°	bad	bad
	10°	bad	bad
Clbeta V	0°	reasonable	reasonable
	5°	bad	bad
	10°	bad	bad
Clbeta WVH	0°	good	good
	5°	good	reasonable
	10°	good	bad
Clbeta WBVH	0°	good	good
	5°		good
	10°		good
CNbeta B	0°	bad	reasonable
	5°		reasonable
	10°		good
CNbeta V	0°	good	good
	5°	reasonable	reasonable
	10°	bad	reasonable
CNbeta WVH	0°	good	good
	5°	good	good
	10°	good	good
CNbeta WBVH	0°	good	reasonable
	5°		reasonable
	10°		reasonable

	Dynamic derivatives		
	Alpha	XFLR5	OpenVSP
Clp V	0°		good
	5°		bad
	10°		bad
Clp WBVH	0°	good	good
	5°		good
	10°		good
CYp V	0°		good
	5°		bad
	10°		bad
CYp WBVH	0°	good	bad
	5°		bad
	10°		bad
CNp V	0°		good
	5°		reasonable
	10°		bad
CNp WBVH	0°	bad	reasonable
	5°		bad
	10°		bad
CYr WBVH	0°	good	reasonable
	5°		reasonable
	10°		reasonable
Clr WBVH	0°	bad	bad
	5°		bad
	10°		bad
CNr WBVH	0°	good	good
	5°		reasonable
	10°		reasonable

	Control derivatives	
	Alpha	XFLR5
Cl Aileron	0°	bad
	5°	bad
	10°	bad
CN Aileron	0°	bad
	5°	bad
	10°	bad
Cl Rudder	0°	reasonable
	5°	bad
	10°	bad
CN Rudder	0°	good
	5°	reasonable
	10°	reasonable
CY Rudder	0°	reasonable
	5°	reasonable
	10°	reasonable

Figure 81 – Summary of results

5. Conclusion

The lateral directional stability and control derivatives of the defined NASA-CRM aircraft were evaluated by semi empirical, vortex lattice and panel method. The method compiled/proposed by Roskam [18] was used as the semi empirical method. XFLR5 software was used for vortex lattice method, combined with panel method for fuselage in the configurations that the fuselage was present. For the wing, this method includes viscous effects by providing 2D data of the airfoils using XFoil [22] simulations. For the panel method OpenVSP was used and no viscous effect is considered. All the methods were calculated for a Reynolds number of 35 million and Mach number of zero.

Semi empirical method was set as reference for comparison as the numerical results presented here are not expected to be the state of art regarding what is possible to achieve within the methodologies and software. Another point for this decision, was that the NASA-CRM aircraft is within the semi-empirical methodology validation range.

Regarding the stability derivatives, a detailed breakdown of the effects was presented and although large discrepancies of results were found during component contribution analysis, the complete aircraft configuration derivatives presented a better agreement between methodologies. The differences for XFLR5 in respect to the semi empirical method for $C_{l\beta WBVH}$ was -13% at Alpha = 0° in respect to the semi-empirical method. OpenVSP results presented between -1% and +7% agreement with the semi-empirical for this derivative. For $C_{N\beta WBVH}$ XFLR5 presented -21% for Alpha = 0° and OpenVSP results between -17% and -26%. For $C_{Y\beta WBVH}$ the differences were larger for XFLR5 which presented between -41% at Alpha = 0°. OpenVSP presented good agreement with values about -7%. All values are presented in respect to the semi-empirical method.

Taking the defined thresholds as reference, it can be said that a regular user of OpenVSP is able to achieve good agreement with semi-empirical method for $C_{l\beta WBVH}$ and reasonable agreement for $C_{N\beta WBVH}$ and $C_{Y\beta WBVH}$. For XFLR5 good agreement can be achieved for $C_{l\beta WBVH}$, reasonable agreement for $C_{N\beta WBVH}$. XFLR5 $C_{Y\beta WBVH}$ presented bad agreement with semi-empirical method, mainly associated with the fuselage side force simulation as seen in the component breakdown.

For dynamic derivatives OpenVSP panel method simulations were performed for the complete configuration (WBVH) while vortex lattice method (XFLR5) was evaluated only considering lifting surfaces and limited to angle of attack of 0°. For the main dynamic derivatives, C_{lp},C_{Yr} and C_{Nr} , XFLR presented results between -4% and -11% and OpenVSP between -9% and -27%. For the secondary dynamic derivatives both methods presented larger differences in respect to the semi-empirical method. As those derivatives values are usually smaller in terms of magnitude the percentage difference reached values above 100%. In any case it does not mean that the impact in flight simulation would be large. For C_{Np} XFLR5 presented +127% difference, while OpenVSP was between -23% and +39% For C_{Yp} XFLR5 presented -15% difference, while OpenVSP was between -43% and -233%. For C_{Rr} XFLR5 presented -60% difference, while OpenVSP was between -51% and -53%. All values are presented in respect to the semi-empirical method. For the main dynamic stability derivatives XFLR5 presented good results and OpenVSP reasonable results. For the secondary dynamic stability derivatives, the results agreement with the semi-empirical method were bad.

For the control derivatives only vortex lattice method was used. Differences in the main aileron($C_{laileron}$) and rudder($C_{Nrudder}$ and $C_{Yrudder}$) derivatives were larger than expected, being +40% (bad agreement), -18% (reasonable agreement) and -19% (reasonable agreement) respectively. No clear reason for the difference was identified.

If it is possible to present a final conclusion about the above described it should be that the numerical methods may be used with care by a regular user. Especially regarding $C_{Y\beta WBVH}$ in XFLR5, probably because of lack of representative fuselage side force. It worth highlighting that use of fuselage is not recommended by the software. For the control derivatives, especially the aileron, it was expected a

better agreement because the vortex lattice method should be able to capture adequately the effect. The reasons for the discrepancy were not identified.

6. Future work

One possibility that could be interesting for the use of vortex lattice method, regarding numerical simulations limitations in respect to the real aerodynamic flow and also aiming for small computational resources, would be to use this method for the lifting surfaces together with semi-empirical methods for accounting the fuselage effect.

As presented in section 4.1 the mesh convergence and simulation setup was not depicted in detail, especially for OpenVSP panel method. A more accurate analysis of this simulation may lead to better simulation standards in order to achieve more consistent results. This detailed analysis was out of the scope of the presented work.

For the 6DOF model continue development spoiler will be defined and a flapped configuration added to the model. It is expected that experimental data from NASA CRM high lift configuration will be available soon and used together with semi-empirical method for the completion of the flight dynamics model.

References

[1] Vassberg, John and Dehaan, Mark and Rivers, Melissa and Wahls, Richard, *Development of a common research model for applied CFD validation studies.*26th AIAA applied aerodynamics conference,2008.

[2] Vassberg, J, *Challengers and Accomplishments of the AIAA CFD Drag Prediction Workshop Series*,AVT-246 Specialists' Meeting on Progress and Challenges in Validation Testing for Computational Fluid Dynamics, Avila, Spain, 2016.

[3] Blumenthal, Brennan and Elmiligui, Alaa A and Geiselhart, Karl and Campbell, Richard L and Maughmer, Mark D and Schmitz, Sven, *Computational investigation of a boundary layer ingestion propulsion system for the common research model*,46th AIAA Fluid Dynamics Conference,2016.

[4] Rivers, Melissa and Dittberner, Ashley, *Experimental investigations of the nasa common research model in the nasa langley national transonic facility and nasa ames 11-ft transonic wind tunnel*, 49th AIAA aerospace sciences meeting including the new horizons forum and aerospace exposition, 2011.

[5] , Zilliac, Greg and Pulliam, Thomas and Rivers, Melissa and Zerr, Jordan and Delgado, Maureen and Halcomb, Nettie and Lee, Henry, *A comparison of the measured and computed skin friction distribution on the common research model*, 49th AIAA Aerospace Sciences Meeting including the New Horizons Forum and Aerospace Exposition, 2011.

[6] , Melissa, B, *Rivers, Support System Effects on the NASA Common Research Model*, AIAA 2012-0707, 2012.

[7] Rivers, Melissa B and Dittberner, Ashley, *Experimental investigations of the NASA common research model*,Journal of Aircraft,2014.

[8] Koga, Seigo and Kohzai, Masataka and Ueno, Makoto and Nakakita, Kazuyuki and Sudani, Norikazu, *Analysis of NASA common research model dynamic data in JAXA wind tunnel tests*,51st AIAA Aerospace Sciences Meeting Including the New Horizons Forum and Aerospace Exposition, 2013.

[9] Kohzai, Masataka and Ueno, Makoto and Koga, Seigo and Sudani, Norikazu, *Wall and support interference corrections of NASA common research model wind tunnel tests in JAXA*, 51st AIAA Aerospace Sciences Meeting Including the New Horizons Forum and Aerospace Exposition, 2013.

[10] Ueno, Makoto and Kohzai, Masataka and Koga, Seigo and Kato, Hiroyuki and Nakakita, Kazuyuki and Sudani, Norikazu, *80% scaled NASA Common Research Model wind tunnel test of JAXA at relatively low Reynolds number*, 51st AIAA Aerospace Sciences Meeting including the New Horizons Forum and Aerospace Exposition, 2013.

[11] Quix, Harald and Hensch, Ann-Katrin, *Dynamic Measurements on the NASA CRM Model tested in ETW*,53rd AIAA Aerospace Sciences Meeting, 2015.

[12] Levy, David W and Laflin, Kelly R and Tinoco, Edward N and Vassberg, John C and Mani, Mori and Rider, Ben and Rumsey, Christopher L and Wahls, Richard A and Morrison, Joseph H and Brodersen, Olaf

P and others, *Summary of data from the fifth computational fluid dynamics drag prediction workshop*, Journal of Aircraft, 2014.

[13] Tinoco, Edward N and Brodersen, Olaf P and Keye, Stefan and Laflin, Kelly R and Feltrop, Edward and Vassberg, John C and Mani, Mori and Rider, Ben and Wahls, Richard A and Morrison, Joseph H and others, *Summary data from the sixth AIAA CFD drag prediction workshop: CRM cases*, Journal of Aircraft, 2018.

[14] Atinault, O and Hue, D, *Design of a vertical tail for the CRM configuration*, GEN, 2014.

[15] Cartieri, Aurelia and Hue, David and Chanzy, Quentin and Atinault, Olivier, *Experimental investigations on the common research model at ONERA-S1MA-comparison with DPW numerical results*, 55th AIAA Aerospace Sciences Meeting, 2017.

[16] Cartieri, Aurelia and Hue, David and Chanzy, Quentin and Atinault, Olivier, *Experimental Investigations on Common Research Model at ONERA-S1MA–Drag Prediction Workshop Numerical Results*, Journal of Aircraft, 2018.

[17] Cartieri, Aurelia, *Experimental investigations on the Common Research Model at ONERA-S2MA*, AIAA Scitech 2020 Forum, 2020.

[18] Roskam, Jan, *Airplane design*, DARcorporation, 1985.

[19] Williams, John E and Vukelich, Steven R, *USAF stability and control digital datcom. volume II. implementation of datcom methods*, MCDONNELL DOUGLAS ASTRONAUTICS CO ST LOUIS MO, 1979.

[20] Wolowicz, Chester H and Yancey, Roxanah B, textitLateral-directional aerodynamic characteristics of light, twin-engine, propeller driven airplanes, NASA TN D-6946, 1972.

[21] McDonald, Robert A, *Advanced modeling in OpenVSP*,16th AIAA Aviation Technology, Integration, and Operations Conference, 2016.

[22] Drela, Mark, *XFOIL: An analysis and design system for low Reynolds number airfoils*,pages 1-12 from book *Low Reynolds number aerodynamics*,1989.

Copyright Statement